Calhoun: The NPS Institutional Archive

DSpace Repository

Theses and Dissertations | 1. Thesis and Dissertation Collection, all items

2018-06

FEASIBILITY AND UTILITY OF AIRBORNE SOLID-STATE LASERS AGAINST GROUND ORDNANCE

Fasone, Joseph

Monterey, CA; Naval Postgraduate School

http://hdl.handle.net/10945/59654

This publication is a work of the U.S. Government as defined in Title 17, United States Code, Section 101. Copyright protection is not available for this work in the United States.

Downloaded from NPS Archive: Calhoun

http://www.nps.edu/library

Calhoun is the Naval Postgraduate School's public access digital repository for research materials and institutional publications created by the NPS community. Calhoun is named for Professor of Mathematics Guy K. Calhoun, NPS's first appointed -- and published -- scholarly author.

Dudley Knox Library / Naval Postgraduate School
411 Dyer Road / 1 University Circle
Monterey, California USA 93943

NAVAL POSTGRADUATE SCHOOL

MONTEREY, CALIFORNIA

THESIS

FEASIBILITY AND UTILITY OF AIRBORNE SOLID-STATE LASERS AGAINST GROUND ORDNANCE

by

Joseph Fasone

June 2018

Thesis Advisor: Keith R. Cohn
Co-Advisor: Joseph A. Blau

Approved for public release. Distribution is unlimited.

THIS PAGE INTENTIONALLY LEFT BLANK

REPORT DOCUMENTATION PAGE			*Form Approved OMB No. 0704-0188*

Public reporting burden for this collection of information is estimated to average 1 hour per response, including the time for reviewing instruction, searching existing data sources, gathering and maintaining the data needed, and completing and reviewing the collection of information. Send comments regarding this burden estimate or any other aspect of this collection of information, including suggestions for reducing this burden, to Washington headquarters Services, Directorate for Information Operations and Reports, 1215 Jefferson Davis Highway, Suite 1204, Arlington, VA 22202-4302, and to the Office of Management and Budget, Paperwork Reduction Project (0704-0188) Washington, DC 20503.

1. AGENCY USE ONLY *(Leave blank)*	**2. REPORT DATE** June 2018	**3. REPORT TYPE AND DATES COVERED** Master's thesis

4. TITLE AND SUBTITLE FEASIBILITY AND UTILITY OF AIRBORNE SOLID-STATE LASERS AGAINST GROUND ORDNANCE	**5. FUNDING NUMBERS**
6. AUTHOR(S) Joseph Fasone	
7. PERFORMING ORGANIZATION NAME(S) AND ADDRESS(ES) Naval Postgraduate School Monterey, CA 93943-5000	**8. PERFORMING ORGANIZATION REPORT NUMBER**
9. SPONSORING / MONITORING AGENCY NAME(S) AND ADDRESS(ES) N/A	**10. SPONSORING / MONITORING AGENCY REPORT NUMBER**

11. SUPPLEMENTARY NOTES The views expressed in this thesis are those of the author and do not reflect the official policy or position of the Department of Defense or the U.S. Government.

12a. DISTRIBUTION / AVAILABILITY STATEMENT Approved for public release. Distribution is unlimited.	**12b. DISTRIBUTION CODE** A

13. ABSTRACT (maximum 200 words)

Explosive devices present a significant threat to civilian populations and are a severe counter-mobility obstacle for ground forces. With the proliferation of improvised explosive devices into potential U.S. military operating areas, a safer and more efficient method for eliminating the threat is required. U.S. Army forces operating at the brigade and above echelons are generally supported with a variety of unmanned aerial vehicle (UAV) airframes that are capable of conducting reconnaissance and surveillance. These UAVs are faster and more responsive to reports of ground-based explosive devices than explosive ordnance disposal (EOD) teams or route clearance patrols. If UAVs were equipped with a system capable of disarming or destroying explosive devices, the stress on EOD assets would be mitigated and the delaying effect of said explosives on ground forces would be reduced. This research explores the feasibility and utility of using a high-energy laser mounted onboard a UAV platform to defeat ground-based explosive devices. Specifically, this research defines an array of potential targets, characterizes the atmospheric effects in varied weather conditions and climates on such a laser system, and contrasts the size, weight, and power requirements of such a system with the operating capabilities of existing UAV platforms.

14. SUBJECT TERMS high-energy laser, unmanned aerial vehicle, UAV, explosive device, high explosives, land mine, improvised explosive device, IED, unexploded ordnance, route clearance, solid-state Laser, airborne platform	**15. NUMBER OF PAGES** 79
	16. PRICE CODE

17. SECURITY CLASSIFICATION OF REPORT	**18. SECURITY CLASSIFICATION OF THIS PAGE**	**19. SECURITY CLASSIFICATION OF ABSTRACT**	**20. LIMITATION OF ABSTRACT**
Unclassified	Unclassified	Unclassified	UU

NSN 7540-01-280-5500 Standard Form 298 (Rev. 2-89) Prescribed by ANSI Std. 239-18

THIS PAGE INTENTIONALLY LEFT BLANK

Approved for public release. Distribution is unlimited.

FEASIBILITY AND UTILITY OF AIRBORNE SOLID-STATE LASERS AGAINST GROUND ORDNANCE

Joseph Fasone
Captain, United States Army
BS, United States Military Academy, 2009

Submitted in partial fulfillment of the
requirements for the degree of

MASTER OF SCIENCE IN APPLIED PHYSICS

from the

NAVAL POSTGRADUATE SCHOOL
June 2018

Approved by: Keith R. Cohn
Advisor

Joseph A. Blau
Co-Advisor

Kevin B. Smith
Chair, Department of Physics

THIS PAGE INTENTIONALLY LEFT BLANK

ABSTRACT

Explosive devices present a significant threat to civilian populations and are a severe counter-mobility obstacle for ground forces. With the proliferation of improvised explosive devices into potential U.S. military operating areas, a safer and more efficient method for eliminating the threat is required. U.S. Army forces operating at the brigade and above echelons are generally supported with a variety of unmanned aerial vehicle (UAV) airframes that are capable of conducting reconnaissance and surveillance. These UAVs are faster and more responsive to reports of ground-based explosive devices than explosive ordnance disposal (EOD) teams or route clearance patrols. If UAVs were equipped with a system capable of disarming or destroying explosive devices, the stress on EOD assets would be mitigated and the delaying effect of said explosives on ground forces would be reduced. This research explores the feasibility and utility of using a high-energy laser mounted onboard a UAV platform to defeat ground-based explosive devices. Specifically, this research defines an array of potential targets, characterizes the atmospheric effects in varied weather conditions and climates on such a laser system, and contrasts the size, weight, and power requirements of such a system with the operating capabilities of existing UAV platforms.

THIS PAGE INTENTIONALLY LEFT BLANK

TABLE OF CONTENTS

LIST OF FIGURES

LIST OF TABLES

THIS PAGE INTENTIONALLY LEFT BLANK

LIST OF ACRONYMS AND ABBREVIATIONS

ABL	Airborne Laser
ALL	Airborne Laser Lab
ATL	Advanced Tactical Laser
AV	anti-vehicle
BCT	brigade combat team
EFP	explosively formed penetrator
GADS	Global Aerosol Data Set
HEAT	high explosive anti-tank
HEL	high energy laser
HMX	high melting explosive
IED	improvised explosive device
LaWS	Laser Weapon System
LEEDR	Laser Environmental Effects Definition and Reference
MIRACL	Mid-IR Advanced Chemical Laser
MTHEL	Mobile Tactical High Energy Laser
NACL	Navy ARPA Chemical Laser
Nd:YAG	neodymium yttrium aluminum garnet
RDX	research department explosive
SBL	Space Based Laser
SWaP	size, weight, and power
THEL	Tactical High Energy Laser
TNT	trinitrotoluene
TOW	tube-launched optically-tracked wire-guided
UAV	unmanned aerial vehicle
UXO	unexploded ordnance

THIS PAGE INTENTIONALLY LEFT BLANK

ACKNOWLEDGMENTS

I’d like to thank my advisors, Professors Keith Cohn and Joseph Blau, for their vast knowledge, assistance, advice, and patience throughout this research. There wasn’t a problem that they couldn’t help with, and they were always a step ahead of me on this project.

To my wife, Erin, who is my greatest friend, supporter, and editor. I couldn’t imagine a better partner in life. Thank you for always helping me to keep it in perspective and not sweat the little things.

Lastly, to my two beautiful daughters, Ava and Louise. You both remind me every day how blessed I am to be a father. Each day is filled with wonderment as your mother and I watch you grow up (but not too fast)!

THIS PAGE INTENTIONALLY LEFT BLANK

I. INTRODUCTION

Explosive devices are among the most effective obstacles to ground maneuver in combat. Properly placed, these devices can inflict casualties, deny terrain, steal operational tempo, and threaten civilian populations. According to figures in 2008, approximately 70% of the then 4,163 U.S. combat deaths in Iraq since the start of the war in 2003 were due to roadside bombs [1]. Their proliferation and successes over the past decade ensure that improvised explosive devices (IEDs), land mines, and unexploded ordnance (UXO) remain a threat in future U.S. Army operating environments.

A. GROUND ORDNANCE THREATS

Relative to the weapons used in modern armed forces, IEDs are cheaply produced and readily available to insurgent or terrorist organizations. A bomb maker might expend less than $100 for an IED capable of destroying a light vehicle as compared to more than $100,000 for a conventional U.S. precision munition [2]. Simply put, organizations that employ IEDs are obtaining a comparable tactical effect for a fraction of what the U.S. government pays per application, and they are doing so without the billions of dollars poured into the acquisition and production of new weapon systems.

Land mines and UXO have a detrimental effect on both combat operations and civilian populations. Like IEDs, these munitions excel in the counter-mobility role against ground forces. However, once they have been bypassed, land mines and UXO still present a significant threat to civilian populations in the vicinity. As of 2003, Soviet land mines from the war in Afghanistan that ended in 1989 still inflicted approximately 300 civilian casualties per month [3]. Unfortunately, even modern armed forces continue to leave behind these dangerous explosives due to limited disposal assets and competing priorities. Apart from the broader humanitarian argument, this threat presents a more immediate challenge to the U.S. Army if the mission specifically entails protection of the civilian population.

B. CURRENT REMOVAL METHODS

Ground-based explosive devices are undoubtedly a problem that the U.S. Army needs to solve safely, effectively, and cheaply in order to be successful on future battlefields. Current removal methods rely on the use of highly specialized units and equipment that may not always be available and are expensive to field. Directed energy is a potential solution to the threat posed by these devices. The Department of Defense recognized the utility of lasers on the battlefield as far back as the 1960s [2] and has since committed funding to multiple projects as a means of combatting a variety of threats to friendly forces.

C. POTENTIAL ADVANTAGES OF DIRECTED ENERGY EMPLOYMENT

In 2004 the U.S. Army demonstrated that in-flight mortar rounds can be destroyed using a ground-based high energy laser. The Mobile Tactical High Energy Laser (MTHEL) destroyed seven medium in-flight mortars during testing, which included a three-round salvo [4]. In 2008 the U.S. Special Operations Command mounted a 100 kW laser on an AC-130 gunship and dubbed it the Advanced Tactical Laser (ATL). The ATL was intended to function as a direct fire weapon against ground targets, which included a remotely controlled vehicle in one particularly successful test [5]. Finally, in 2010 the U.S. Air Force succeeded in destroying an in-flight ballistic missile using the Airborne Laser (ABL), a megawatt-class laser mounted inside a Boeing 747 [5] (Figure 1).

Figure 1. YAL-1A Airborne Laser. Source: [6].

Although the MTHEL, ATL, and ABL were successful during testing in ideal conditions, all three projects were cancelled for the same general reasons. Each system utilized a large chemical laser that, aside from the massive size (the MTHEL required several oversized trailers to move across the battlefield [5]), required the transportation, storage, and handling of dangerous and expensive chemicals. Additionally, each project was built on the assumption that the laser would be in the right location at the right time to strike a fast moving target. In the case of the ABL, five to seven Boeing 747s would have to maintain a presence near a missile launch site for a successful interdiction [5]. Such a quantity of large, slow aircraft loitering over enemy controlled territory would be an irresistibly attractive target. In order for directed energy to be successful in tactical engagements, lasers must be smaller, logistically simple, and mobile.

This study models the use of solid-state lasers mounted on unmanned aerial vehicles (UAVs) against surface-laid ground ordnance. Solid-state lasers operate by electricity instead of chemical reactions and are generally much smaller than chemical lasers. Current solid-state lasers also produce much less optical output power than their chemical relatives, but this may be offset by the intended application. While the MTHEL, ATL, and ABL required high irradiance over a short dwell time to be successful, a solid-state laser that targets ground ordnance has the luxury of an extended engagement period

since IEDs, land mines, and UXO don't move. Additionally, the explosives used in these potential targets self-ignite at temperatures of a few hundred kelvins; this is considerably lower than the temperatures needed for other target types (e.g., to melt through missile casings). Thus, the irradiance, and consequentially the output power, of the laser can be reduced while still achieving the desired effect.

UAVs are ideal platforms for destroying ground ordnance with solid-state lasers. Currently, a brigade combat team (BCT) in the U.S. Army fields four RQ-7B Shadow UAVs that are intended to provide 24-hour geographic coverage for that BCT's area of operations. The availability of UAVs only increases at each higher echelon, with the MQ-1C Gray Eagle (Figure 2) fielded at the division-level. This means that there is a persistent and flexible UAV presence within every area of operations that could potentially put a laser at the right location and time to be effective against the ground ordnance threat. Additionally, UAVs have a large stand-off distance from ground targets that eliminates the need to put soldiers or expensive equipment within the blast radius of said ground ordnance. The challenge for using UAVs in this intended application lies in the fact that all of these platforms have limited capacity for the size, weight, and power (SWaP) requirements inherent to solid-state lasers.

Figure 2. MQ-1C Gray Eagle. Source: [7].

Aside from the engineering challenges associated with mounting lasers on UAVs, an air-to-ground directed energy system must consider atmospheric propagation effects such as diffraction, scattering, absorption, and turbulence [2]. Consequentially, the required beam output power must be designed to overcome these effects and cross the lethal fluence threshold at the target.

D. OVERVIEW OF STUDY

This study identifies the energetic compounds used in common IEDs, surface-laid land mines, and pieces of UXO in order to estimate the lethal fluence needed for these compounds. Based on this information, the study then estimates the laser power needed to achieve the lethal fluences over acceptable dwell times for various atmospheric conditions. Finally, the study discusses the feasibility of using solid-state lasers against ground ordnance based upon SWaP considerations and UAV platform availability.

THIS PAGE INTENTIONALLY LEFT BLANK

II. OVERVIEW OF DIRECTED ENERGY WEAPONS

As it is applied to weaponry, the term “directed energy” can have a multitude of meanings. For example, the deposition of energy on a target can be accomplished through the use of microwaves, particle beams, or high energy lasers (HELs). However, for directed energy weapons to be effective, the delivery method, target parameters, platform allowances, and propagation medium must be such that the desired result on the target is achieved. HELs are currently a highly active subject of study for defense applications and will be the focus for this research due to their relative advantages over other types of directed energy weapons.

A. HISTORY

The development of HELs as weapons began almost immediately following the invention of the first laser in 1960. The Soviet Union started researching the feasibility of HELs defeating intercontinental ballistic missiles during their reentry phase in 1965, going so far as establishing a town of 20,000 people at Raduga to conduct research and testing [8]. The United States followed when Ed Gerry created a gas dynamic CO2 laser with an output power of 100 kW in 1968 [8]. Each branch of the armed forces began funding their own projects tailored for their specific requirements.

The next major advancement came from the U.S. Navy with the creation of the Navy ARPA Chemical Laser (NACL), which was a multi-hundred kilowatt-class chemical laser. The NACL successfully destroyed tube-launched optically-tracked wire-guided (TOW) missiles in-flight in 1978 and led to the development of the Mid-IR Advanced Chemical Laser (MIRACL) in 1980, which was the world’s first megawatt-class laser [9]. However, chemical lasers are not ideal for ship-based applications due to the fuels required and exhaust they create. Additionally, the less-than-ideal output wavelength produced by these lasers were prone to atmospheric absorption, which resulted in decreased irradiance at the target and thermal blooming. These factors contributed to a hiatus in Navy HEL design until a suitable alternative with comparable power outputs could be developed. In 2014, the 30 kW AN/SEQ-3 Laser Weapon System (LaWS) (Figure 3) was installed on

the USS *Ponce* and successfully demonstrated the ability to destroy small boats and UAVs [10]. The LaWS is a solid-state system that circumvents the challenges of chemical lasers at the expense of an output that is lower by at least an order of magnitude.

Figure 3. LaWS Onboard the USS *Ponce*. Source: [11].

The U.S. Air Force created the Airborne Laser Lab (ALL) with a 100 kW class gas dynamic laser mounted in a KC-135 aircraft, which succeeded in destroying AIM-9 missiles and BQM-34 drones during testing in 1983 [8]. Due to the relatively low electrical power requirements of chemical lasers, this type of system was the basis of the Space Based Laser (SBL) program that began in 1989 with the purpose of defeating ICBMs in their boost phase. The program intended to conduct a successful demonstration by 2012 [9], but was cancelled in 1991 [8]. Building on the successes of the ALL and prompted by the cancellation of the SBL, the Air Force began work on the ABL program in 1994, which incorporated a megawatt class laser in a Boeing 747 [8]. As mentioned in the previous chapter, the ABL was successful during testing in its intended purpose of destroying ballistic missiles in the boost phase, but the requirement of putting the laser within range of a target and program costs led to its cancellation.

Meanwhile, the U.S. Army took an interest in using ground-based HELs to counter indirect fire. Research for the Tactical High Energy Laser (THEL) began in 1996 as a joint venture between the United States and Israel as a means to interdict Katyusha rockets [9]. The THEL achieved successes in testing against rockets in 2000 and against mortar rounds in 2004, but proved too expensive and unwieldy on the battlefield. The THEL and its offshoot, the MTHEL, were cancelled due to a lack of available funding. Although the Army lost interest in the THEL and MTHEL, it did not lose interest in ground-based HEL applications and by March 2003 deployed the Zeus HMMWV Laser Ordnance Neutralization System (Figure 4) to Afghanistan to assist with UXO removal [12]. That version of the Zeus incorporated a 500 W neodymium yttrium aluminum garnet (Nd:YAG) solid-state laser [9] with an effective range of 300 meters [12]. During its six-month deployment to Bagram Air Field, the Zeus negated over 200 pieces UXO, including a record-breaking 51 pieces of UXO in less than 100 minutes [12]. The performance of the Zeus demonstrated the feasibility of using a HEL to destroy ground ordnance.

Figure 4. Zeus HMMWV Laser Ordnance Neutralization System. Source: [13].

Nearly 60 years of HEL design and testing revealed several lessons regarding their use as weapons. Although chemical and gas lasers are capable of achieving higher output powers at relatively better efficiencies, they are also unwieldy, if not downright dangerous to the user in battlefield applications. Solid-state lasers are currently receiving the most attention due to innovations that have increased their power output, their safer electrical "fuel," and their ideal wavelength for atmospheric propagation. This research will focus primarily on solid-state systems due to these reasons, especially considering the projected application of using them onboard UAVs. As the Zeus device demonstrated, only modest output power is needed to affect the desired result against ground ordnance.

B. ADVANTAGES AND DISADVANTAGES

Solid-state HELs have numerous advantages when compared to conventional ballistic weapons. Perhaps the most significant is that the beam propagates at the speed of light. The next major advantage of HELs is the cost per engagement associated with using the weapon. Ballistic munitions are expensive and only available in limited quantities; armored vehicles, aircraft, and ships can only carry a finite number of rounds, bombs, or missiles. On the other hand, lasers only cost the fuel required to generate electricity for each engagement; a typical cost of less than a dollar compared to thousands of dollars for conventional munitions. Finally, HELs can generally outrange conventional line-of-sight munitions if the laser is designed to overcome the effects of scattering and absorption that lead to beam extinction.

Solid-state HELs do come with some inherent disadvantages that have so far prevented their widespread deployment. Compared to ballistic munitions and chemical or gas lasers, solid-state HELs are inefficient. The typical "wall-plug" efficiency for solid-state systems is on the order of 20% to 30%, which necessitates an electrical power source capable of providing hundreds of kilowatts for each engagement. This inefficiency leads to heat generation in the lasing medium that must be actively removed. Cooling systems that can effectively dissipate the heat add additional power and weight requirements. Additionally, any HEL system is more susceptible to atmospheric effects, such as precipitation and haze, than conventional ballistic munitions. Since the defeat mechanism

employed by HELs typically involves heating of the target, a laser must also overcome the energy loss resulting from light reflected by the target's surface.

Considering the objective of this research, airborne HELs are an attractive option for defeating explosive devices. If explosive ordnance disposal (EOD) personnel decide that a device can be rendered ineffective in-situ, there are a variety of methods available that include disruptors, anti-munition rifles, de-armers, explosives, fuze removal, or fuze immunization [14]. All of these options require deployment of EOD teams and potentially place these specially trained personnel at risk (Figure 5). Simply the loss of time incurred by friendly forces is often enough to justify the emplacement of explosive devices by the enemy. By requiring friendly forces to adjust from a proactive posture to a reactive one, an enemy that employs these devices steals the tactical initiative. Conversely, HELs (particularly airborne systems) enable the discoverer of an explosive device to act expeditiously and with pinpoint precision. Barring prohibitive weather conditions, UAVs continuously occupy the airspace of a U.S. Army unit's area of operations. The operational cost in time incurred by a friendly unit that encounters an explosive device could potentially be cut from hours (waiting on an EOD team or combat engineers to arrive) to minutes (the time it takes to direct an already airborne clearance asset to the location). This is not to say that using airborne HELs to dispose of explosive devices completely negates the need to have EOD assets available; weather occasionally grounds UAVs, disposing of a device in-situ is not always a possibility, and it is likely infeasible to use a HEL to defeat buried devices. However, it does provide another option for ground commanders to leverage based on the merits of the tactical situation.

Figure 5. EOD Personnel Train to Dispose of an IED. Source: [15].

C. PROJECTED APPLICATIONS

HEL systems have demonstrated success in testing and limited field deployments, and the next generation of these weapons are currently in the design phase. The Navy established their Directed Energy Program Office within the Program Executive Office for Integrated Warfare Systems in August 2016 [16]. In a February 2017 Federal Business Opportunities posting, this office requested industry capabilities for a new program that consists of a 60 kW HEL with counter-ISR dazzling capability and is capable of operating on an Arleigh Burke-class guided missile destroyer [16]. The Air Force is currently funding a demonstration called SHIELD, which intends to integrate a solid-state HEL with an output power in the tens of kilowatts range on a fighter-size aircraft by 2020 [17]. The Army is investing in its High Energy Laser Mobile Demonstrator, a ground-based system primarily intended to counter indirect fire and UAVs and is capable of being transported by a relatively small armored vehicle such as a Stryker personnel carrier [18]. All of these projects underline the increased interest in HEL weapons, particularly solid-state systems, and the great advances that have been made in HELs since the first laser was invented in 1960.

III. CHARACTERIZATION OF HIGH EXPLOSIVE TARGETS

Land mines, UXO, IEDs, and most other high explosive devices share the same basic components and principles of operation. It is this similarity that enables a single clearing system, such as a HEL, to be effective against a wide range of potential threats. Accordingly, three different explosive devices serve as target profiles for this research: the TM-83 anti-vehicle (AV) land mine, the PTAB-2.5M high explosive anti-tank (HEAT) sub-munition, and a Composition C-4 based IED. These devices were selected due to how well they characterize each category of munition (surface-laid land mine, UXO, and IED, respectively), current usage, and variety in construction and materials. This chapter will describe the fundamental components of high explosive devices and will detail the defeat mechanism selected for their removal using a HEL.

A. COMPOSITION

Explosive devices generally consist of four basic components; the detonator, the booster charge, the main charge, and the casing. The detonator is the component that triggers a detonation and can come in many forms. Conventional munitions such as bombs and artillery shells that are commonly found as UXO contain a fuze or a timer for this purpose. Land mines and IEDs make use of switches, sensors, wired detonators, or wireless receivers (Figure 6). Regardless of the form, the detonator is ultimately what initiates an explosive reaction in the booster charge.

Figure 6. IEDs Captured in Afghanistan with Detonators Mounted on Top. Source: [19].

Booster charges are an intermediary material between the detonator and the main charge. Detonators usually do not provide enough energy to trigger an explosive reaction in the most common types of high explosives, so a less stable explosive is used to create a shock wave that will detonate the main charge. The main charge is what gives a device its explosive power and is usually the largest internal component (Figure 7). Common military-grade explosives used for main charges include trinitrotoluene (TNT), research department explosive (RDX), and high melting explosive (HMX). Perhaps the most commonly used combination of these explosives is Composition B-3, which is a 60% RDX and 40% TNT mixture [20].

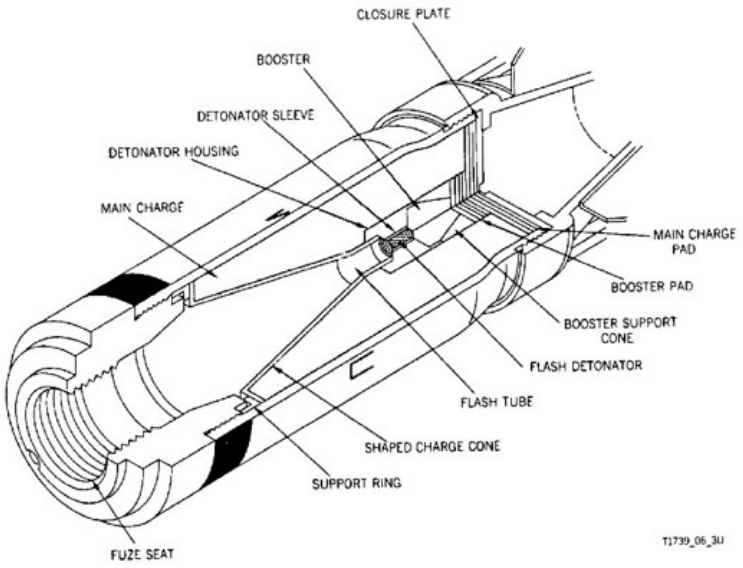

Figure 7. Cross-sectional Diagram of a PTAB-2.5M HEAT Sub-munition Depicting Booster and Main Charges. Source: [21].

The final basic component found in most explosive devices is the casing. The number of combinations of materials, shapes, and fragmentation patterns found in casings is effectively limitless. Metal casings provide durability and double as shrapnel when the device detonates, but are easier to detect with the magnetic scanners commonly employed by clearing assets. Conversely, plastic casings are difficult to detect, but require more care during handling and must be filled with some form of shrapnel to maximize effectiveness. Of particular note is the modern use of the explosively formed penetrator (EFP), which is a circular concave piece of malleable metal (usually copper) that is mounted over the main charge. Upon detonation, the explosive forces reshape the metal into a molten dart-like projectile capable of penetrating most types of armor. The TM-83 AV land mine is an example of a device that produces an EFP (Figure 8).

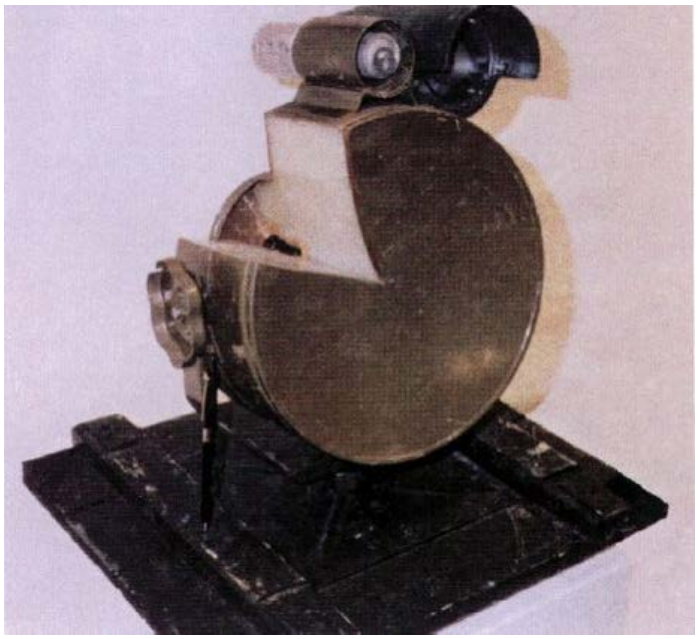

Figure 8. TM-83 AV Land Mine with Triangular Cutout Exposing Main Charge. Source: [22].

B. HIGH EXPLOSIVE PROPERTIES

The potential energy of an explosive material is analogous to a boulder resting on the edge of a cliff [23]. Initially, a great deal of energy is expended to move the boulder to this position. For explosives, this is referred to as the heat of formation. Once the boulder is at the edge, only a slight nudge is required to push it over and expend the high potential energy stored within. Accordingly, this nudge is known as the activation energy. The relatively rapid expenditure of energy during this detonation is what differentiates explosives from other high-energy materials such as wood, coal, or oil. In the case of coal versus HMX, the power output is a difference of nine orders of magnitude [23].

In this research, the "nudge" is the defeat mechanism used to destroy the designated targets. The HEL acts as an energy pump by depositing a portion of its energy in the form of heat on the surface of the target (the rest of its energy is reflected depending on the surface material). As the HEL deposits more energy over time, the temperature of the casing rises as heat diffuses through it and ultimately reaches the main charge contained

within. The heat transfer in both the casing and main charge is easily modeled with the well-known heat diffusion equation:

$$\rho c_p \frac{\partial T}{\partial t} = \nabla \cdot (\kappa \nabla T) \tag{1}$$

where ρ is the density of the casing or main charge, c_p is the specific heat capacity, T is the temperature, and κ is the thermal conductivity. Once the interface between the casing and main charge reaches an explosive property known as the autoignition temperature, the main charge will begin expending its potential energy in a manner similar to the falling boulder. While this mechanism will not produce a full detonation, it will render the explosive device ineffective by forcing the main charge to deflagrate [24]. This removal method can actually be more favorable than full detonation if the explosive device is located in close proximity to valuable infrastructure or populated areas.

C. EFFECT OF HEATING

As heat deposited by the laser beam accumulates at the interface between the casing and the main charge, the explosive material will undergo a chemical reaction and release its stored potential energy in the form of additional heat. The rate at which the explosive releases heat as it undergoes the chemical reaction is known as the thermal rate constant. While the constant is initially a relatively small value, it will grow exponentially as the heat deposited by the HEL combines with the accumulating heat emitted by the explosive. The empirical Arrhenius Law is probably the oldest yet best-known model for expressing this thermal rate constant *k(T)* [25]:

$$k(T) = Ae^{-\frac{E}{k_B T}} \tag{2}$$

where A is a pre-exponential constant, E is the activation energy, k_B is the Boltzmann constant, and T is the temperature of the explosive material. The pre-exponential constant is unique to a given chemical reaction and is often determined experimentally with units similar to the thermal rate constant (with magnitude typically on the order of 10^{10}) [26]. When the temperature is low, this pre-exponential factor is suppressed. However, as the temperature of the explosive rises relative to its activation energy, the extremely large pre-exponential factor causes the thermal rate constant to increase dramatically. The complete

model for predicting heat transfer in an explosive material is a combination of both the heat diffusion equation (Equation 1) and the Arrhenius Law (Equation 2) and appears as:

$$\rho c_p \frac{\partial T}{\partial t} = \nabla \cdot (\kappa \nabla T) + \rho Q Z e^{-\frac{E}{k_B T}} \tag{3}$$

where Q is the heat of decomposition and Z is the characteristic reaction rate of the explosive [27]. The product of the explosive's density, heat of decomposition, and characteristic reaction rate is the pre-exponential constant A annotated in Equation 2. The Arrhenius term acts as a heat source in the heat diffusion equation. Once the temperature T reaches the autoignition temperature, the Arrhenius term dominates and acts as a "positive feedback loop," producing a "run-away" reaction. The predicted autoignition temperature for Composition B-3 is approximately 800-K [20], while the predicted value for Composition C-4 is approximately 650-K [20].

IV. LASER BEAM PROPAGATION THROUGH THE ATMOSPHERE

The environment through which a laser beam propagates can dramatically affect the beam's properties from origin to termination. The Earth's atmosphere is full of molecules and particles that can influence a laser beam, and this fact must be accounted for in any system that intends to propagate over a meaningful distance. This chapter will describe those effects as well as their impact on an airborne laser system engaging ground-based targets.

A. VACUUM PROPAGATION

Before considering the effects of atmosphere on beam propagation, it is first necessary to understand how a beam propagates under ideal conditions. Due to the wave nature of light, any light source directed through an aperture will experience divergence. This will cause the radius of the beam, known as the beam waist, to increase in accordance with the divergence angle (Figure 9).

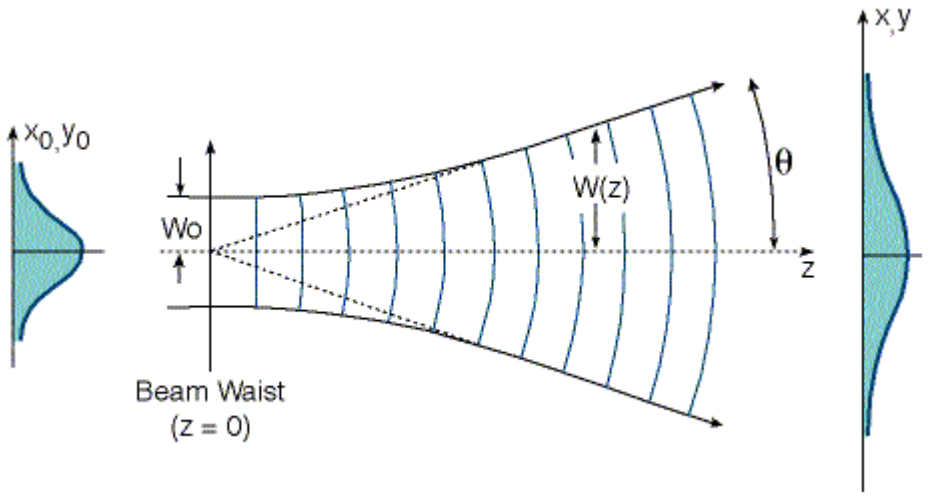

The divergence angle is represented by θ. Note the Gaussian profiles in the margins depicting the decrease in beam irradiance as propagation distance increases.

Figure 9. Beam Waist *w* as a Function of Propagation Distance *z*. Source: [28].

The beam waist size, divergence angle, and beam wavelength determine the quality of the laser beam. This parameter is known as the beam quality factor and is calculated with the equation:

$$M^2 = \frac{w_0 \pi \theta}{4\lambda} \tag{4}$$

where M^2 is the beam quality factor, w_0 is the beam waist size, θ is the divergence angle, and λ is the beam wavelength [29]. A beam quality factor of 1 indicates an ideal Gaussian irradiance profile. However, current lasers are not perfect and will produce beams with a factor greater than 1. The greater the value of the beam quality factor, the less irradiant the laser beam will be at the target. For this research, a beam quality factor of 3 is used for simulations in order to produce more realistic results.

The size of the laser beam director itself can also significantly impact the qualities of the beam. The effect of beam director diameter on beam waist can be approximated with the equation:

$$w_0 \approx M^2 \left(\frac{2\lambda z}{\pi D} \right) \tag{5}$$

where w_0 is the beam waist size, M^2 is the beam quality factor, λ is the beam wavelength, z is the propagation distance, and D is the beam director diameter [30]. As the beam director diameter increases, the beam waist will decrease and produce a more irradiant beam profile at the target. However, regarding the use of lasers on airborne platforms, it is necessary to keep the beam director as small as possible due to limited space availability and payload capacity. In these simulations, the beam director diameter is set at 25 cm in order to accurately represent a system capable of being mounted to a UAV.

B. EXTINCTION

Atmospheric extinction of a laser beam is the result of two separate phenomena. The first of these is absorption, in which atmospheric molecules and aerosol particles absorb incoming photons and thereby decrease the irradiance of the laser beam. Absorption is dependent on the wavelength of the photons and the types of particles present. Since Earth's atmosphere is composed of numerous varieties of molecules and particles, there are only a few narrow wavelength bands that are favorable for beam propagation. Many

solid-state lasers currently designed for directed energy applications have wavelengths near 1 μm, which is within a "window" in which light propagates with minimal absorption.

The second effect that causes beam extinction is scattering. Particles in the atmosphere with sizes comparable to the wavelength of light will deflect light rays in random directions. This effect is evident in white clouds, in which water vapor scatters incident light with wavelengths across the visible spectrum. Particles generated as dust or by pollution also scatter light, resulting in a hazy atmosphere (Figure 10).

Figure 10. Haze Created by Atmospheric Scattering of Light by Aerosol Particles. Source: [31].

Laser beam extinction is modeled as an exponential decay. The Beer-Lambert Law provides the mathematical foundation with the function:

$$P(z) = P_0 e^{-\varepsilon z} \tag{6}$$

where *P(z)* is the beam's power as a function of propagation distance, *z* is the propagation distance, P_0 is the initial power, and ε is an extinction coefficient that accounts for wavelength-specific scattering and absorption information and also depends on location, time of day, aerosol concentration, etc. [32]. For the intended application of defeating explosive devices, the extinction coefficient must be as small as feasible, which is largely

accomplished by selecting a beam wavelength of approximately 1 μm that tends to minimize extinction (Figure 11).

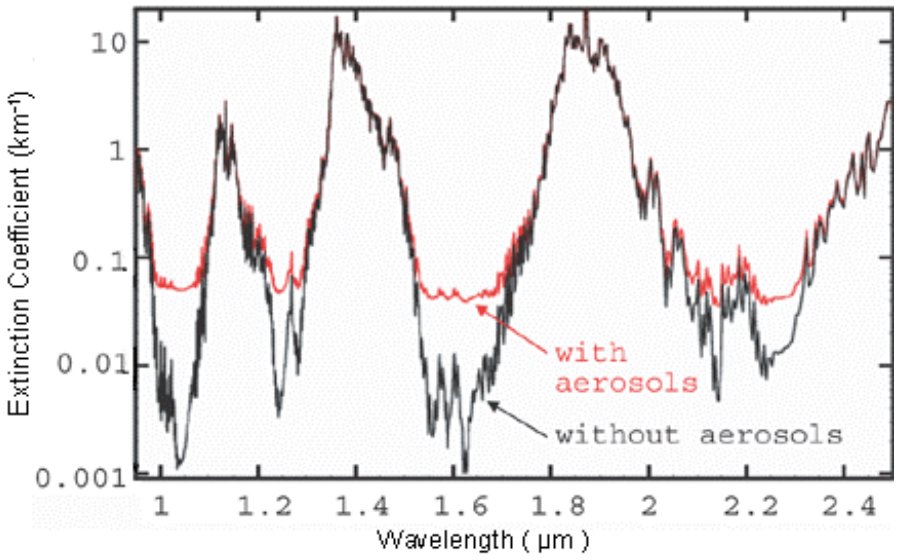

The red plot includes the presence of aerosols. Note the relatively low extinction coefficient values at approximately 1 μm and 1.6 μm.

Figure 11. Effect of Wavelength on Beam Extinction. Source: [33].

C. TURBULENCE

As the sun's radiation heats the atmosphere and Earth's surface, it creates differences in air temperature. Accordingly, these cells of air have different densities and pressure that alter their optical indices of refraction. When a light ray transmits between different cells, variations in the indices of refraction cause the light ray to deflect. In addition to this deflection, turbulent cells that are smaller than the laser beam's cross-sectional area will cause portions of the beam to diverge. This divergence results in a loss of coherence, as portions of the beam become out of phase and destructively interfere with each other. The ultimate consequence of turbulence is a distorted, larger, and less intense time-averaged beam spot on the target.

Turbulence is quantified by the refraction structure parameter C_n^2, which is a measure of the change in the air's index of refraction over distance:

$$C_n^2 = \frac{\overline{[n(x) - n(x+r)]^2}}{r^{2/3}} \quad (7)$$

where *n(x)* is the index of refraction and *n(x+r)* is the index of refraction at range *r* [34]. A value of 10^{-14} $m^{-2/3}$ indicates stronger turbulence, while a value of 10^{-17} $m^{-2/3}$ indicates weaker turbulence.

The refraction structure parameter is of little analytical value by itself, but can be used to estimate the effect of turbulence on beam coherence at the target. The Fried parameter is an estimation of the diameter over which a laser beam maintains transverse coherence throughout a desired propagation distance:

$$r_0 = [0.423(2\pi / \lambda)^2 \int_0^z C_n^2(z)dz]^{-3/5} \quad (8)$$

where r_0 is the Fried parameter, λ is the wavelength, and z is the propagation distance [32]. This formula incorporates C_n^2 along the beam path. As the value of C_n^2 increases, the value of the Fried parameter decreases. For example, given a beam wavelength of 1 μm, a constant C_n^2 value of 10^{-14} $m^{-2/3}$, and a propagation distance of 3 km, the Fried parameter would be approximately 2.4 cm. Under these conditions, any laser beam that is greater than 2.4 cm at its source (established by the beam director diameter) will be significantly affected by turbulence (Figure 12).

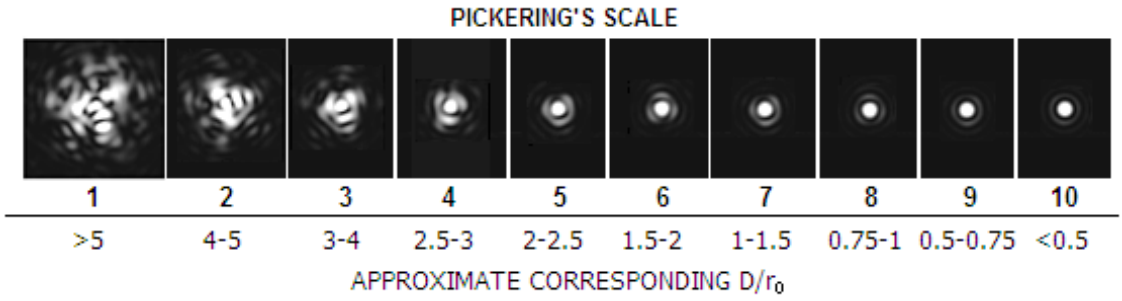

Pickering's scale provides a visual approximation of the relationship between the Fried parameter and beam director diameter (denoted as *D*). Each scale number corresponds to a representation of a beam cross-sectional area. As D/r_0 becomes greater than 1, the beam's area will increase and break apart.

Figure 12. Pickering's Scale. Source: [35].

D. THERMAL BLOOMING

A laser beam itself can modify the properties of the air it is propagating through. As photons are absorbed by aerosols and molecules along the beam path, energy is released in the form of heat. This heat in turn alters the air's index of refraction by causing the air to expand and become less dense. As the beam continues to propagate through this modified air, it will begin to diverge more quickly than would otherwise be expected via this thermal blooming process [32]. This phenomenon is highly susceptible to temperature-altering effects such as wind. If wind blows across a beam path that is experiencing thermal blooming, it will cool the incident side of the beam and push heated air to the opposite side. The beam will then "bend" into the cooler, and therefore denser, side of the "lens" (Figure 13).

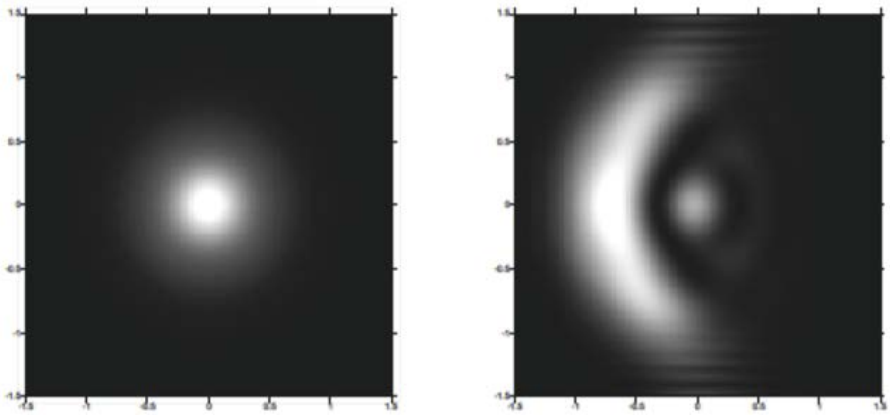

The image on the left depicts a beam profile without wind, while the image on the right depicts beam "bending" caused by a wind blowing from left to right.

Figure 13. Effect of Wind on Thermal Blooming. Source: [36].

Thermal blooming is roughly characterized through a dimensionless thermal distortion factor, N_t:

$$N_t = \frac{-(dn/dT)}{n\rho c_p} \times \frac{KIz^2}{vr} \tag{9}$$

where n is the air's index of refraction, (dn/dT) is the rate of change in the index of refraction as a result of temperature change, ρ is the air's density, c_p is the heat capacity of

the air, *K* is the absorption coefficient of the air, *I* is the laser beam's irradiance without thermal blooming, *z* is the distance of propagation, *r* is the beam's radius, and *v* is the crosswind's speed [32]. A larger thermal distortion factor indicates greater beam distortion and decreased intensity at the target. If the crosswind speed or beam radius increase, the thermal distortion number will decrease. However, increasing beam irradiance or propagation distance has the unwanted effect of increasing the thermal distortion number. Figure 14 depicts the effect that the thermal distortion number has on the relative intensity of the laser beam.

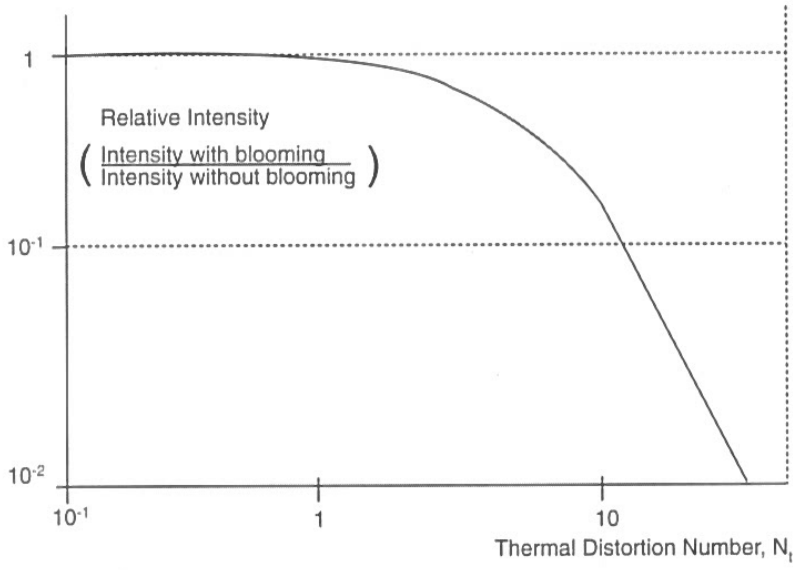

Figure 14. Relationship between Thermal Distortion Number and Relative Intensity. Source: [32].

E. ELEVATION EFFECTS

Using a HEL on an airborne platform to engage ground-based targets has several advantages relative to ground-based lasers. Turbulence is often dramatically reduced at elevation since the platform is further from the ground, and consequently, further from heat sources and surface effects (Figure 15). Although the laser beam is still required to propagate through low-altitude atmosphere as it nears the target, the path over which turbulence is a factor is greatly diminished and restricted to the terminal portion. A ground-

based laser beam must suffer the effect over its entire path, including at the beam's origin where it has the greatest effect on the rest of propagation.

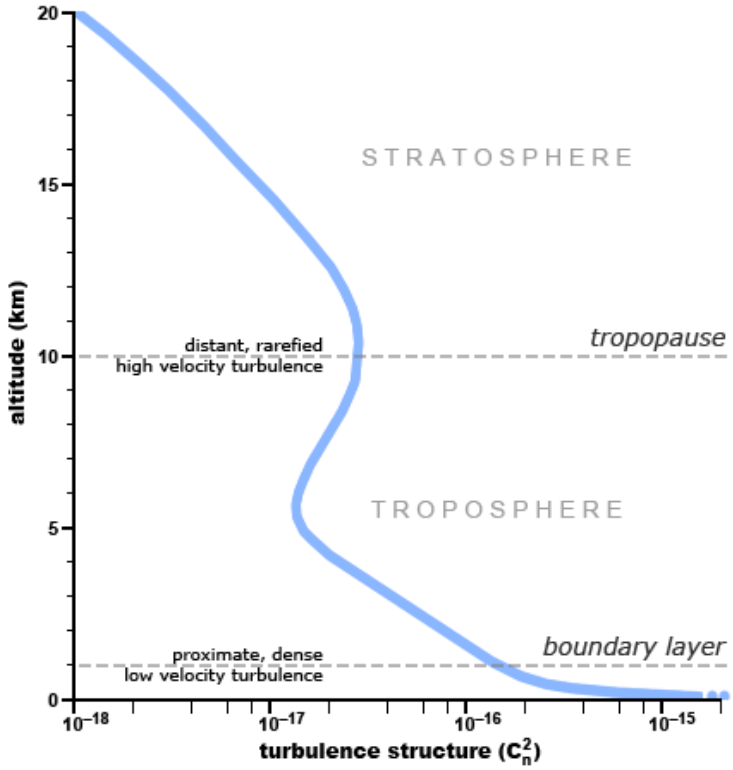

Smaller UAVs operate at lower altitude (approximately 2 km) while larger UAVs operate at higher altitude (between 15 km and 18 km).

Figure 15. Effect of Altitude on Atmospheric Turbulence. Source: [37].

Additionally, air density decreases with altitude, which exponentially decreases absorption and increases beam irradiance at the target. The desire to use UAVs as the airborne platform of choice in this research also introduces an advantage regarding thermal blooming. All UAVs currently employed by the U.S. Army are fixed wing aircraft that cannot remain stationary in flight. This means that any laser beam originating from a UAV platform will constantly be moving through unheated air and experience a relative wind proportional to the velocity of the UAV itself. These two factors effectively eliminate thermal blooming as a consideration for the intended application of this research.

V. METHODOLOGY

This research simulates air-to-ground laser engagements of ground ordnance using computer-based MATLAB code with user-defined parameters. This chapter will address the variety of parameters used and the reasons for their selection. It will also identify existing simulations used, upon which this research is partially based.

A. TARGET PARAMETERS

Three different types of ground ordnance are modeled in this research: a land mine, IED, and piece of UXO. While it would be impossible to model every explosive device currently in use, the established target profiles emphasize generalized distinctions between the three types. The fundamental differences between these categories are target geometry, outer casing, and explosive material.

1. Geometry

All three types of target have myriad geometries available to choose from. However, the problem can be simplified when approached from the context of this research. Any laser beam intentionally aimed at an object of known range will be deliberately focused in order to reduce its effective area on the target. This focus spot acts as a source term for the heat diffusion equation previously mentioned in Chapter III (Equation 1). The profile of the laser beam is assumed to be a Gaussian distribution modeled by the equation:

$$S = I_{pk}(1-R)e^{-\frac{r^2}{w_{tot}^2}} \tag{10}$$

where S is the source term for the heat diffusion equation, I_{pk} is the peak irradiance of the laser beam, R is the reflectivity coefficient of the target's surface, r is the radial coordinate of the profile, and w_{tot} is the beam waist size. For these simulations, the reflectivity coefficient is assumed to have a value of 0.1, since most explosive devices are intentionally coated in dark non-reflective materials that conceal them within surroundings.

Ideally, the beam waist is minimized at the target due to focusing (although this can be affected by atmospheric conditions). As a characteristic example, the circular face of the TM-83 AV land mine has a radius of 12.5 cm, with a surface area of approximately 490 cm^2 [22]. Assuming that a typical laser beam has a waist of 3 cm at the target and a cross-sectional area of approximately 28 cm^2, it is reasonable to neglect the effect of geometry on the target's heating since the beam area constitutes less than 6% of the total irradiated surface. Therefore, a standard geometry is used for all three target types during simulations, which consists of a right circular cylinder of 10 cm radius and 10 cm height, with one circular surface being irradiated by the laser beam at its center.

2. Outer Casing

There is a wide variety of casing materials used in explosive devices, which principally reduces to the distinction of plastic versus metal. As previously discussed, metal casings provide for safer handling of the device and have the added effect of increasing shrapnel upon detonation. Steel is a commonly used metal for this purpose and is the material used in many military-grade munitions. Due to this fact, it is appropriate to select steel as the outer casing for the land mine and UXO target profiles, since both are characteristically employed by military forces. Since the thickness of these casings is highly variable between specific devices, a generalized thickness of 5 mm is used for the land mine profile, while a thickness of 2.5 mm is used for the UXO profile. As the casing material is the same in both of these profiles, the simulation results illustrate the effect that casing thickness has on the required dwell times.

Plastic casings are more difficult to detect on the battlefield and are readily available to amateur explosives manufacturers, such as the insurgents and terrorists that employ IEDs. Although IEDs can and have been encased with metal, high density polyethylene is used in this research as the outer casing for the IED profile in order to demonstrate the effect that casing material has on required dwell times. A generalized thickness of 5 mm is used for the IED profile in order to make it comparable to the steel-encased land mine profile, also of 5 mm thickness. Table 1 includes a comprehensive listing of the all outer casing thermal property values used during actual simulations.

Table 1. Outer Casing Thermal Properties. Source [38].

Material	Density, ρ [kg/m^3]	Thermal Conductivity, κ [W/(m*K)]	Heat Capacity, c_p [J/(kg*K)]
Steel (Plain)	7854	60.5	434
Polyethylene (High Density)	959	0.43	2000

3. Explosive Material

Since World War II, RDX is one of the most commonly used components in military-grade high explosives. It is a majority ingredient found in several Composition A, B, and C mixtures widely used by U.S. armed forces (up to 98.5% in Composition A-3, 60% in Composition B-3, and 95% in Composition C-3) [20]. Its thermochemical properties are widely studied and publicized, making it a reasonable assumption that most professional and amateur military forces employ it or its derivatives to some extent. This fact makes it an ideal material to include in generalized models of all three target types, and the thermal property values needed to do so are included in Table 2. These parameters are discussed in the context of the heat diffusion equation in Chapter III (Equation 3).

Table 2. RDX Thermochemical Properties. Source [39].

Density, ρ [kg/m^3]	Thermal Conductivity, κ [W/(m*K)]	Heat Capacity, c_p [J/(kg*K)]	Heat of Decomposition, Q [MJ/kg]	Activation Energy, E [kJ/mol]	Characteristic Reaction Rate, Z [s^{-1}]
1800	0.29	2093	2.09	199	$10^{18.5}$

B. ATMOSPHERIC PARAMETERS

In order to establish the atmospheric conditions under which to conduct simulations, it is necessary to consider climate type and weather. Since the combination of these two factors result in a countless number of geographic locations to model, it is necessary to also consider the likelihood that a particular region could become the home of

an armed conflict within the near future. Seoul, South Korea and Kandahar, Afghanistan provide highly contrasting climatic conditions with potential for continuing and future military operations. Seoul possesses a temperate climate [40], which is well distinguished from the arid desert climate of Kandahar [41]. The contrast provided by these locations demonstrates the effect that climate has on the required target dwell times.

With climates established, it is also necessary to specify the exact weather conditions under which the simulations will be performed. In order to exemplify the extremes under which engagements could occur, clear and precipitous weather conditions are modeled. Clear weather enables ideal laser beam propagation, while the presence of large water droplets models the most non-ideal condition under which to engage ground ordnance with a laser. As an intermediary, hazy weather conditions are modeled in order to demonstrate the effect of aerosols on the engagements. All regional atmospheric properties are acquired from the Laser Environmental Effects Definition and Reference (LEEDR) database created at the Air Force Institute of Technology.

C. LASER AND PLATFORM PARAMETERS

Bearing the combined effect of target and atmospheric parameters in mind, the laser and platform configuration is critical in achieving a successful simulated engagement. The four most important parameters in this regard are the laser beam quality, laser beam wavelength, platform altitude, and laser power output.

1. Laser Beam Quality and Wavelength

As previously discussed, laser beam quality has a significant impact on the beam's irradiance at the target. A beam quality factor of 3 is used in these simulations to model a realistic laser. Atmospheric absorption of laser energy is highly dependent on the laser's frequency. In order to minimize absorption, a lasing wavelength of 1.0642 μm is used in these simulations. While other wavelength "windows" exist that minimize absorption, 1 μm is a commonly used wavelength in a multitude of existing solid-state systems.

2. Platform Altitude

The capabilities of the UAV platform are the driving factor in determining the altitude at which the laser will engage the target. Generally, the greater the size and power of a UAV, the greater its maximum operating altitude, or service ceiling, will be. The RQ-7B Shadow, which is the smallest UAV currently used that could potentially carry a laser system, typically operates at an altitude of 2.4 km to 3 km during the day [42]. Conversely, the RQ-4 Global Hawk, which is likely the largest current UAV that could be used in this capacity, has a service ceiling of over 18 km [43].

Since increasing altitude also increases the amount of atmosphere through which the laser beam must propagate, a minimal altitude is ideal for these simulations. Three different altitudes of 1 km, 4 km, and 7 km are considered in this research to provide a reasonable range of values that could accommodate any tactical concerns. While 7 km is certainly not a limit imposed by existing UAV platform capabilities, it is within the upper limit of altitudes that enable engagement dwell times to remain minimal, which is kept within 60 seconds in this research.

3. Laser Power Output

In order to use an airborne platform for these engagements, the laser system must be kept as compact as possible with regard to SWaP design considerations. This is especially significant when the proposed airborne platform is a UAV, which are typically far smaller and less powerful than their manned counterparts or ground-based platforms. Considering the material properties of the proposed targets and the propagation distances of the laser beam, a power output less than 2.5 kW would likely be insufficient to achieve the desired effect, especially at higher altitude and in non-ideal weather conditions.

Fiber lasers are currently a viable solid-state laser option for producing outputs in the kilowatt range while maintaining beam quality and minimizing weight. For example, IPG Photonics, which specializes in producing industrial cutting lasers, manufactures a 1 μm continuous wave ytterbium fiber system with a scalable power output of 1 kW to 10 kW that weighs less than 380 pounds [44]. Such a system would be ideal for providing the necessary power output while minimizing size and weight. Accordingly, this research

considers the effects of a 2.5 kW, 5 kW, and 10 kW power output in order to explore a range of powers likely to be mounted onboard a UAV platform.

D. SIMULATION TOOLS

This research relies on a pair of simulation tools developed at renowned defense research institutions. This section will briefly expound on both the inputs and outputs required to incorporate these tools into the simulated engagements.

1. LEEDR

As mentioned, LEEDR is a database of atmospheric conditions that generates regional approximations for the light propagation coefficients discussed in Chapter IV. LEEDR enables the user to control the weather conditions at specified locations using preset values or averages unique to that particular location. For these simulations, regional weather monitoring stations known as "ExPERT" sites in LEEDR will be used. Incheon International Airport is the ExPERT site representative of Seoul, while Kandahar Air Base is the ExPERT site used for the city of Kandahar. With one exception, all weather profiles used are representative of summer weather conditions (July), with the ambient temperature taken as the daily average for that location. The one exception is the precipitous weather profile for Kandahar since southern Afghanistan typically only receives rain during the winter months, which LEEDR bases on average conditions in the month of January. Clear and hazy profiles utilize a relative humidity percentile setting of 50% (i.e., more humid than 50% of measured days, and so represents a typical humidity for that location in January or July). Precipitous profiles utilize a relative humidity percentile setting of 99%. The widely known Hufnagel-Valley model for turbulence [45] was applied to all profiles as well.

Clear weather profiles utilize a Global Aerosol Data Set (GADS) multiplier of 1, which simulates a typical aerosol concentration for that location. The clear weather profiles do not include any cloud or rain effects. Precipitous weather profiles utilize a GADS multiplier of 0.2, the addition of "moderate rain" (a LEEDR setting that corresponds to 12.5 mm per hour), and a cloud layer at 10 km altitude. While a cloud layer at this height is unrealistic, it enables the simulation to demonstrate the effect of rain throughout the path

of propagation. Otherwise the extinction effect generated by a cloud layer would completely disrupt a laser beam and prevent target autoignition (this effectively makes any simulations performed at 4 km and 7 km platform altitude under precipitous conditions unrealistic and therefore irrelevant). Finally, hazy weather profiles utilize a GADS multiplier of 3, which simulates high aerosol concentration, and do not include any cloud or rain effects. See Table 3 and Table 4 for a complete listing of settings used to generate the LEEDR weather profiles.

Table 3. Seoul Weather Profile Settings.

Weather	Aerosol Model	Aerosol Multiplier	Rain	Season	Temp.	Relative Humidity Percentile
Clear	GADS	1	-	Summer	Daily Avg.	50%
Precipitation	GADS	0.2	12.5 mm per hour	Summer	Daily Avg.	99%
Haze	GADS	3	-	Summer	Daily Avg.	50%

Table 4. Kandahar Weather Profile Settings.

Weather	Aerosol Model	Aerosol Multiplier	Rain	Season	Temp.	Relative Humidity Percentile
Clear	GADS	1	-	Summer	Daily Avg.	50%
Precipitation	GADS	0.2	12.5 mm per hour	Winter	Daily Avg.	99%
Haze	GADS	3	-	Summer	Daily Avg.	50%

2. ANCHOR

Developed at the Naval Postgraduate School, ANCHOR is a scaling code that simulates the effect of atmospheric propagation on a laser beam. Its inputs include the LEEDR weather profile, laser parameters, and platform conditions. Its outputs include the beam waist size and beam irradiance over an array of cross ranges defined by the user. ANCHOR is capable of modeling the effects of extinction, turbulence, and thermal blooming, although the thermal blooming capability is not used in these simulations for the reasons discussed in Chapter IV. For this research, ANCHOR is used as a preliminary simulation for each test case that provides the laser beam parameters at the target prior to and during heat diffusion.

VI. RESULTS AND CONCLUSIONS

This chapter discusses the effect that each independent variable has on required dwell times based on results obtained through simulation. The chapter concludes by determining the capabilities of laser systems with different output powers and the potential for mounting them onboard different UAVs based on SWaP requirements.

A. EXTINCTION PROFILES

Climate and weather conditions dramatically alter the atmospheric effects on laser beam propagation. Specifically, the effects of beam extinction are increased from clear to hazy weather, and even further increased when accounting for the presence of precipitation. See Figure 16, Figure 17, and Figure 18 for LEEDR-generated data regarding the extinction coefficient of various weather types in Seoul, South Korea. For reference, see Table 3 and Table 4 for the settings used to generate these figures.

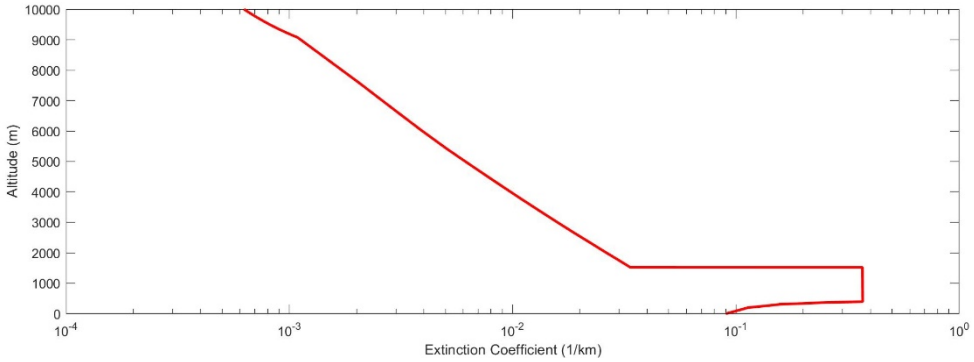

Figure 16. Extinction Coefficient for Clear Seoul Weather Conditions.

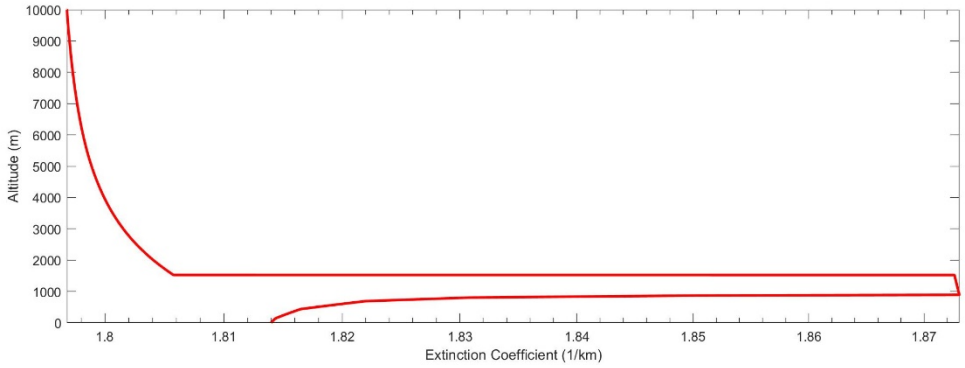

Note the scale used for the extinction coefficient in this figure is linear (unlike the logarithmic scales used Figure 16 and Figure 18).

Figure 17. Extinction Coefficient for Precipitous Seoul Weather Conditions.

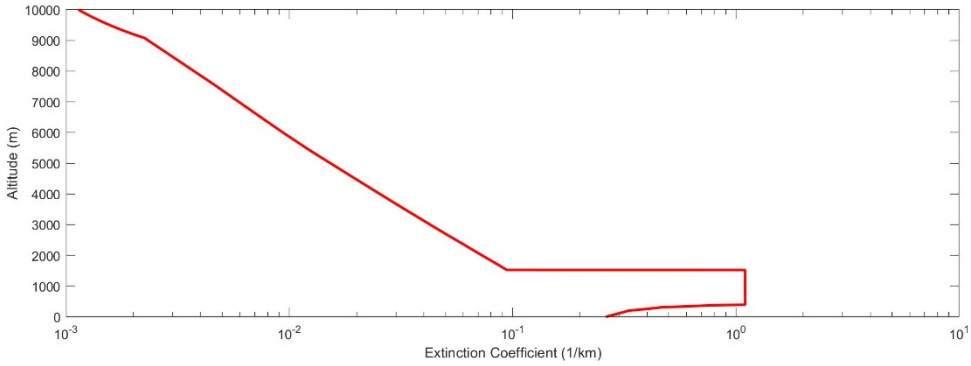

Figure 18. Extinction Coefficient for Hazy Seoul Weather Conditions.

The plots for extinction coefficient share the same general characteristics across both climates and all three weather profiles. From ground-level to an altitude of approximately 1 km (the atmospheric boundary layer), the coefficient value increases. However, just above the boundary layer at approximately 2 km altitude, the coefficient value decreases dramatically and then steadily declines even further with increased altitude. An increase in extinction coefficient value corresponds with a decrease in the amount of laser output power that actually reaches the target in accordance with the Beer-Lambert Law (Equation 6). Of note, the extinction coefficient data for Kandahar, Afghanistan indicates that, for similar weather types, the coefficient value generally remains less than that in Seoul across the platform altitudes simulated. The difference in

extinction coefficient profiles can be explained by the relative abundance of atmospheric moisture near Seoul and the absence thereof near Kandahar. The extinction coefficient is inversely related to the surface visibility generated by LEEDR for each profile. Table 5 displays the effects that climate and weather type have on surface visibility.

Table 5. Effects of Climate and Weather on Surface Visibility.

	Seoul, South Korea			Kandahar, Afghanistan		
	Clear	Precipitation	Haze	Clear	Precipitation	Haze
Surface Visibility (km)	23.7	1.64	8.50	33.3	1.64	12.0

The key conclusion to draw with regard to climate type is that, based on the data for these two locations, drier climates will produce more favorable atmospheric conditions for laser beam propagation (not considering the effects of sand storms). This effect is manifested in universally reduced dwell times for targets engaged in an arid desert environment, even when other independent variables are adjusted. In later sections, the Seoul climate profiles will be used to identify the extreme limits under which target autoignition can occur.

B. EFFECT OF WEATHER

To illustrate the effect of weather type on required dwell time, platform altitude, output power, and target type are kept constant. The comparison in Figure 19 displays data taken from 1 km platform altitude, 2.5 kW output power, and land mine target engagements.

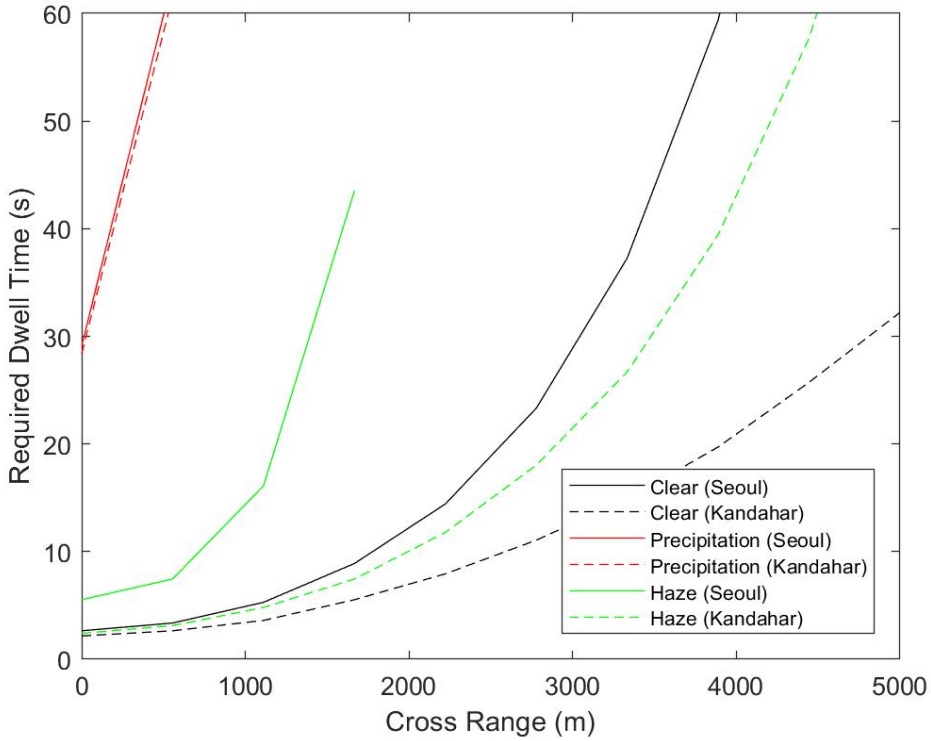

Note that the plot for hazy Seoul weather conditions stops at a cross range of approximately 1.75 km. This is due to the fact that the simulation is unable to achieve autoignition in the target within 60 seconds of dwell time at greater cross ranges.

Figure 19. Simulation Results for 1 km Platform Altitude, 2.5 kW Output Power, Land Mine Target Engagements.

Predictably, clear weather conditions produce the most favorable dwell times. The reduced presence of atmospheric particles corresponds with reduced beam extinction. Hazy weather conditions produce the next lowest dwell times, since the high concentration of aerosols results in increased beam scattering and absorption. Finally, precipitous weather produces the highest dwell times since the presence of large water droplets effectively extinguishes the beam at greater cross ranges.

This data supports the conclusion that, although required dwell times are severely degraded, a low-power 2.5 kW laser is still capable of successfully engaging ground ordnance across all three weather types simulated. In precipitous conditions, the cross range is reduced to approximately 500 m for a 2.5 kW laser system. However, in clear

conditions, the same system can achieve autoignition conditions in the target at a cross range in excess of 5 km.

C. EFFECT OF TARGET TYPE

To illustrate the effect of target type on required dwell times, engagements in clear weather, at 1 km platform altitude, and with 2.5kW output power are considered. See Figure 20 for simulation results.

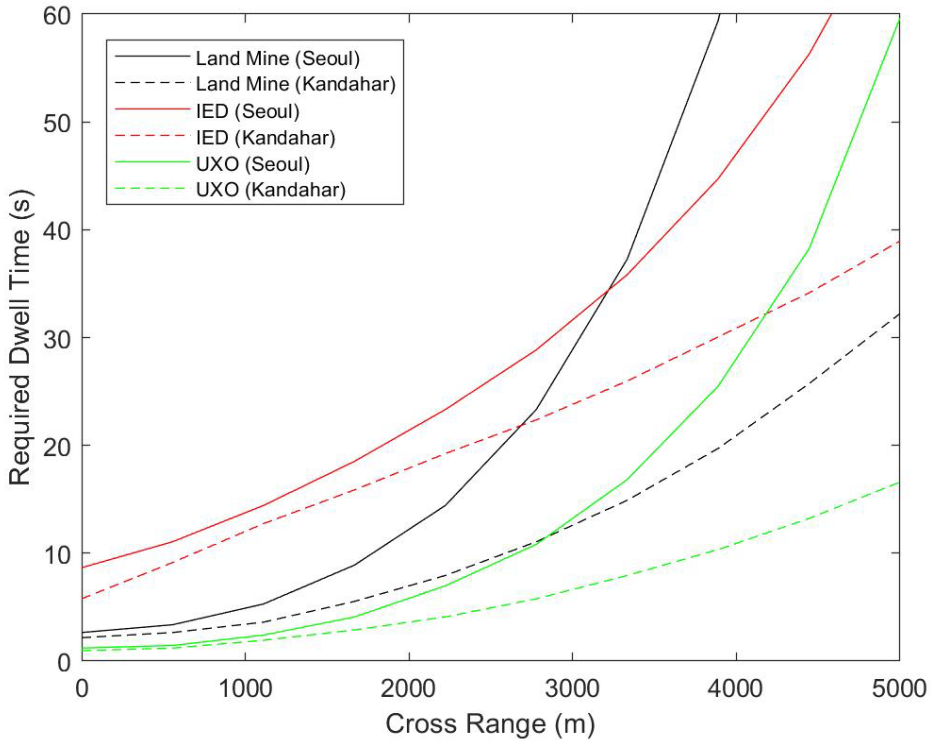

The plots for land mine and IED targets engaged under similar climate conditions (Seoul) intersect at a cross range of approximately 3.25 km, which indicates that the land mine is a more difficult target to defeat at greater cross ranges under these simulation parameters.

Figure 20. Simulation Results for Clear Weather, 1 km Platform Altitude, 2.5 kW Output Power Engagements.

Outer casing thickness has a significant effect on required dwell time. When comparing the two steel-encased targets, the UXO target profile (2.5 mm of casing) universally produces lower dwell times than the land mine target profile (5 mm of casing).

Casing material has an even more dramatic effect on dwell times. The dwell times for the IED target profile, with its 5 mm of high density polyethylene casing, increase exponentially with respect to increasing cross range similarly to the steel-encased targets. However, the rate of this exponential increase is noticeably less than that for the steel profiles. Even though the IED target requires greater dwell times at lower cross ranges, the IED target data intersects the land mine target data at a cross range of approximately 3.25 km in Figure 20, after which the IED profile for Seoul actually requires lower dwell times than the land mine profile (also for Seoul). This intersection is indicative of different heating behaviors for both materials as beam irradiance is affected by increases in the propagation path (Figure 21).

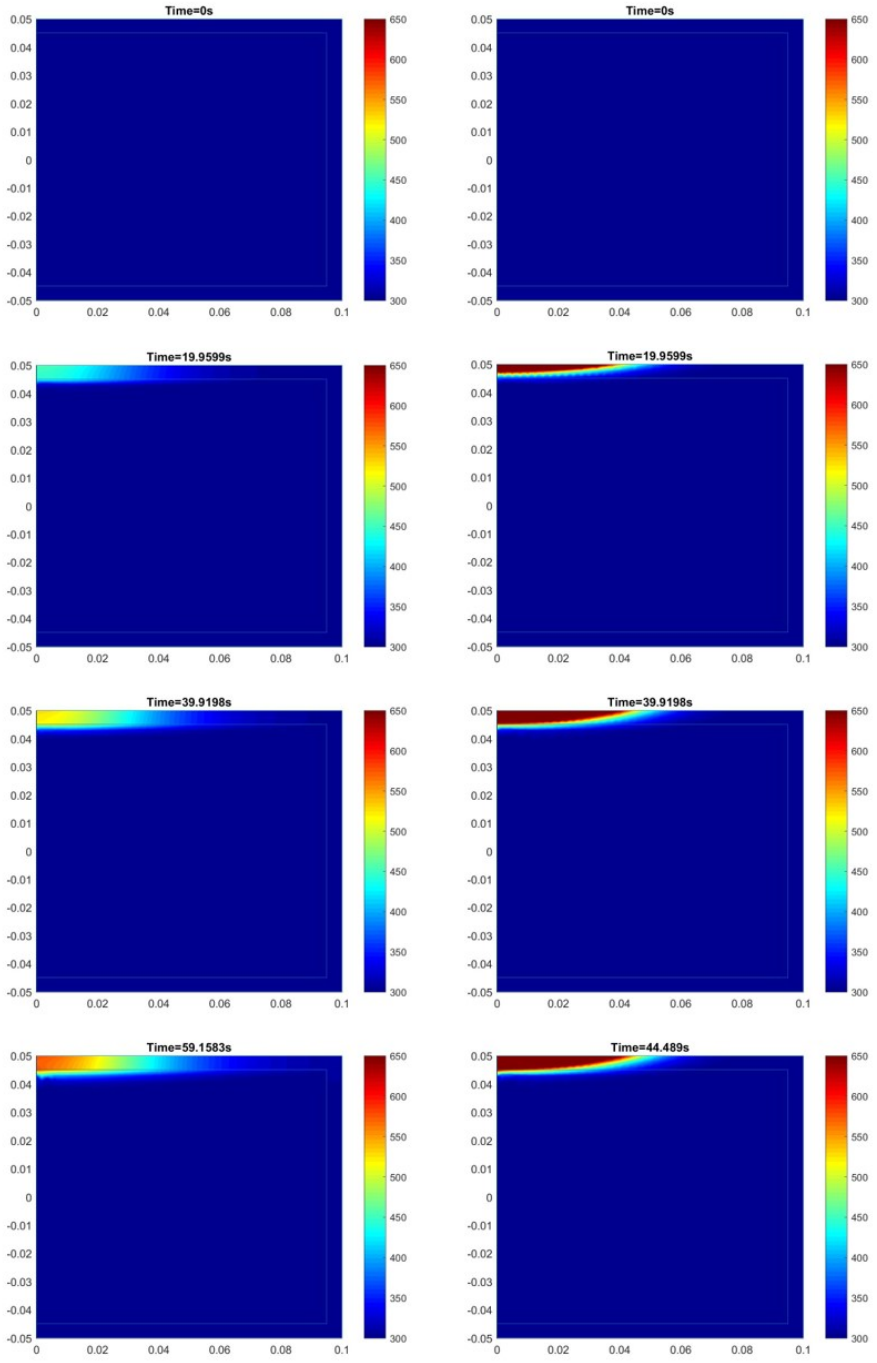

The figures on the left represent heating of a land mine target while the figures on the right represent heating of an IED target. For reference, the axes are in units of meters while the color scale is in units of kelvins. The bottom figure of each target is a depiction of the heating profile immediately prior to autoignition.

Figure 21. Target Cross-sectional Heating in Seoul Climate, Clear Weather, 1 km Platform Altitude, 2.5 kW Output Power, 3.89 km Cross Range Engagements.

Due to the insulating nature of polyethylene, heat deposited by the laser beam remains relatively local to the beam spot on the surface of the target, where it accumulates and diffuses at a faster rate towards the explosive interface than it does radially outward. However, being a conductive material, steel casing diffuses more heat radially outward from the beam spot. When the beam irradiance is high (i.e., when the spot size is small at shorter cross ranges), the heat diffuses rapidly enough in both directions (towards the explosive interface and radially outward) that the target autoignites. When beam irradiance is low (i.e., when the spot size is larger at longer cross ranges), the radial diffusion prevents enough heat from reaching the explosive interface and autoigniting the RDX in a reasonable amount of time.

Since the melt temperature of high density polyethylene ranges between 383 K and 408 K [46], there is concern that the amount of heat deposited by the laser beam will melt the IED target's outer casing prior to explosive autoignition. However, it is possible to approximate the amount of total energy deposited by the laser beam that would be required to achieve such a state transition. The energy required to melt a material that is being irradiated by a laser beam can be approximated using the equation:

$$E_m \approx H_f \rho \pi w_{tot}^2 l \tag{11}$$

where E_m is the required melt energy, H_f is the heat of fusion (245 kJ/kg for high density polyethylene [46]), w_{tot} is the beam waist size, and l is the material thickness. Conversely, the total energy deposited by the laser beam can be approximated as:

$$E_b \approx I_{pk} \pi w_{tot}^2 t_d (1-R) \tag{12}$$

where E_b is the energy deposited by the beam, I_{pk} is the peak irradiance of the beam, t_d is the required dwell time for autoignition, and R is the reflectivity coefficient of the material. Relating Equation 11 and Equation 12 produces the equation:

$$G \approx \frac{H_f \rho l}{I_{pk} t_d (1-R)} \tag{13}$$

where G is the fraction that relates the energy required to melt the casing material to the total energy deposited by the laser beam. Upon conducting this calculation for a sample of simulations, the percentage is approximated to remain below 10% of the total energy deposited by the laser beam. It is therefore a reasonable assumption to neglect the energy

consumed by melting with regard to the time scales and polyethylene casing thickness modeled in these simulations.

In addition to melting, there is concern over the effect imposed by the removal of polyethylene casing while the target is irradiated (either by burning or gravity). In either case, the removal of mass would reduce the time required for the heat front to diffuse in accordance with the heat diffusion equation mentioned in Chapter III (Equation 1). In the case of burning (high density polyethylene itself has an autoignition temperature of approximately 613 K [46]), the energy released by burning the casing would actually contribute to the heat front diffusion. The ultimate effect of casing removal in either situation would be a reduction in the dwell time required to achieve autoignition in the target. Therefore, by not considering the effect of casing removal in this research, the simulation results are likely to be conservative (i.e., higher dwell times) than those that would be achieved through experimentation. Having established that the land mine and IED target types are the most difficult with which to achieve autoignition conditions, they are used as the standards by which to establish the requirements of a laser system intended to defeat ground ordnance.

D. EFFECT OF PLATFORM ALTITUDE

Simulated engagements performed in clear weather, with 2.5 kW output power, and against land mine targets are used to compare the effect of platform altitude on required dwell time (Figure 22).

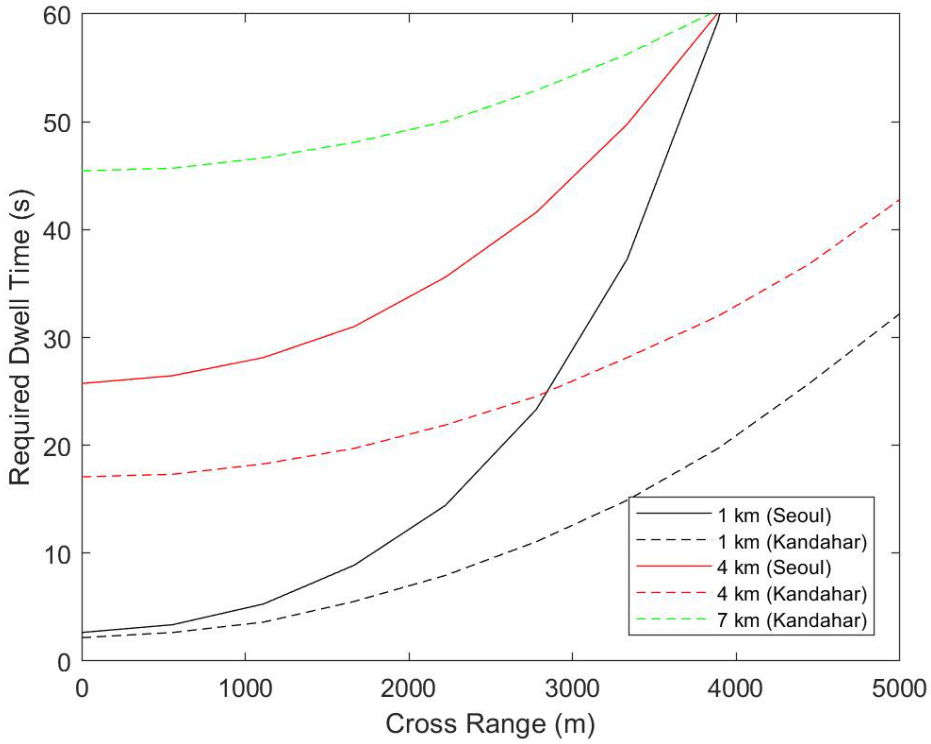

The plot for an engagement in Seoul at 7 km platform altitude is not available since the simulated laser beam is unable to achieve autoignition conditions in the target within 60 seconds of dwell time.

Figure 22. Simulation Results for Clear Weather, 2.5 kW Output Power, Land Mine Target Engagements.

There is a universally strong relationship between platform altitude and the required dwell time to achieve autoignition conditions. This can be explained by the increased effects of scattering, absorption, and turbulence as the propagation path of the laser beam increases. Although lower altitudes result in reduced engagement dwell times, they are also disadvantageous for UAV operations. An aircraft operating at low altitude is more vulnerable to anti-aircraft defenses, and relatively slow-moving UAVs are particularly vulnerable. Since low-level cloud layers typically exist below 2 km altitude [47], the only tactical reason for a UAV to operate below this altitude would be the presence of rain clouds (hence why precipitous weather simulations are relevant at 1 km altitude, but not 4 km or 7 km) or in overcast conditions. However, conducting engagements at high altitude places a tax on the laser system's requirements. Of note, the plots for the 1 km platform altitude and 4 km platform altitude engagements in Seoul converge at a cross range of

approximately 4 km. This can be attributed to the effect of increased extinction coefficient in the atmospheric boundary layer. While the simulation performed at 1 km platform altitude must propagate almost the entire distance with a very large coefficient value, the simulation performed at 4 km platform altitude only propagates through the boundary layer for approximately half of the distance to the target.

E. EFFECT OF OUTPUT POWER

Engagements performed in clear weather, at 1 km platform altitude, and against land mine targets are used to determine the effect of laser output power on required dwell times. See Figure 23 for a visual comparison of the data.

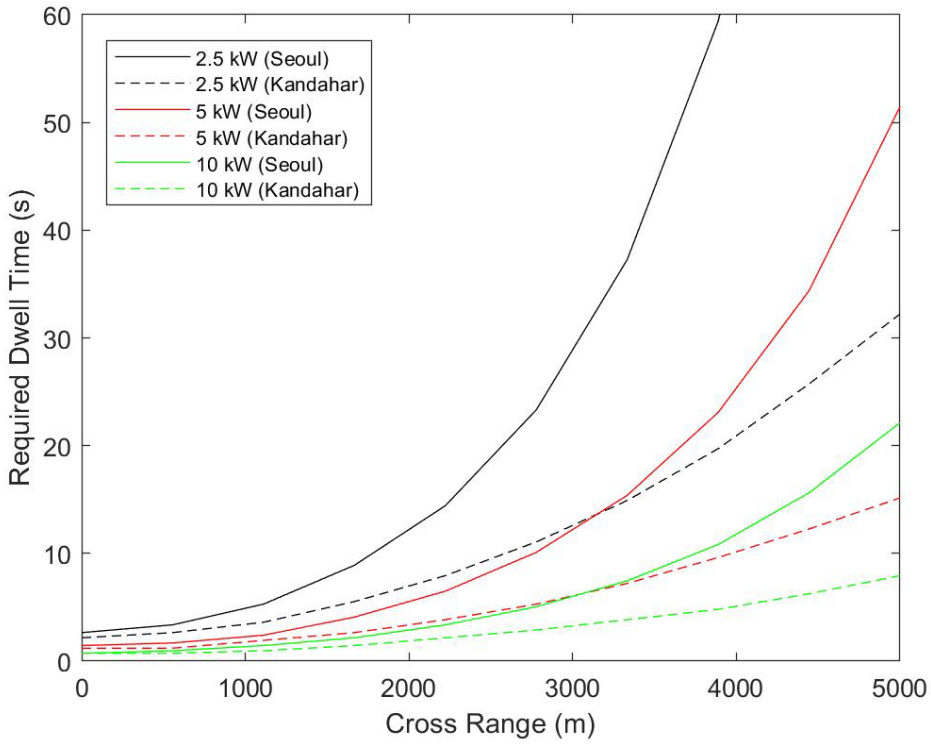

Figure 23. Simulation Results for Clear Weather, 1 km Platform Altitude, Land Mine Target Engagements.

As expected, laser output power plays a significant role in determining the required dwell time. Greater output power means that more energy is deposited at the surface of the

target and consequentially increases the diffusion speed of the heat front through the outer casing. Of all the independent variables tested in this research, laser output power is the most significant with regard to designing a system capable of achieving target autoignition across all conditions.

As identified in previous sections of this chapter, engagements that occur in a temperate climate (Seoul) are non-ideal relative to those that occur in a drier climate (Kandahar). Additionally, depending on the platform altitude, precipitous and hazy weather are the most disruptive weather conditions regarding laser beam propagation. Finally, land mine and IED target types are the most difficult to defeat. These conclusions enable identification of the maximum capabilities of the three simulated output powers. A temperate climate with precipitous weather at 1 km platform altitude is the most non-ideal situation under which a 2.5 kW output power can achieve autoignition in the two most difficult target types (Figure 24).

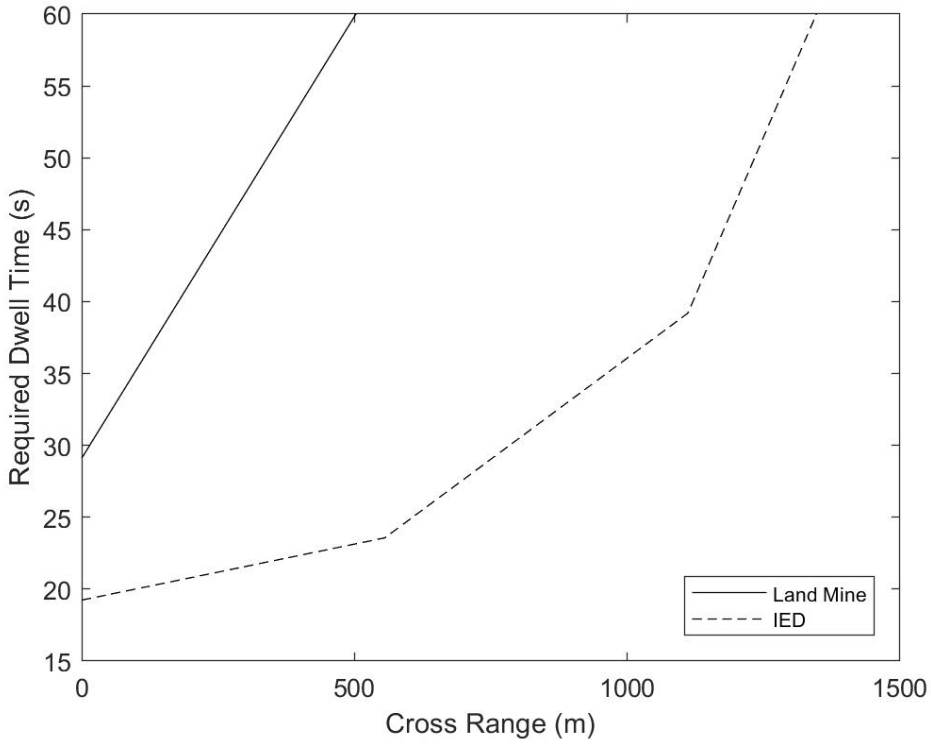

Figure 24. Simulation Results for a Seoul Climate, Precipitous Weather, 1 km Platform Altitude, 2.5 kW Output Power Engagement.

Increasing the output power of the laser to 5 kW enables target autoignition at a platform altitude of 4 km in hazy weather conditions (Figure 25).

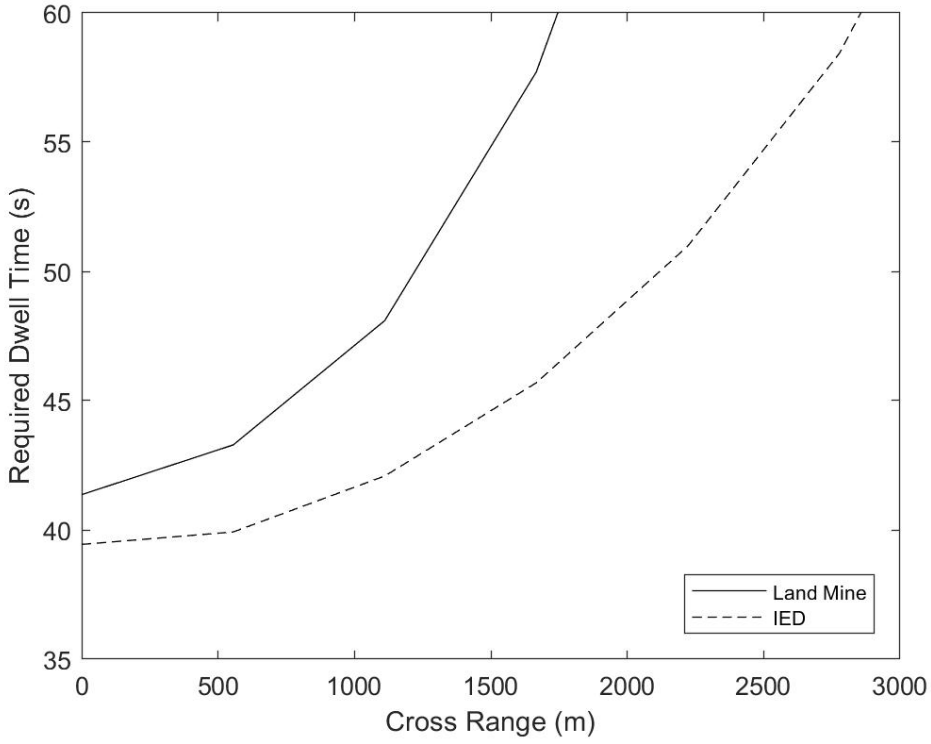

Figure 25. Simulation Results for a Seoul Climate, Hazy Weather, 4 km Platform Altitude, 5 kW Output Power Engagement.

Finally, the maximum simulated output power of 10 kW enables target defeat at a platform altitude of 7 km in hazy weather conditions (Figure 26).

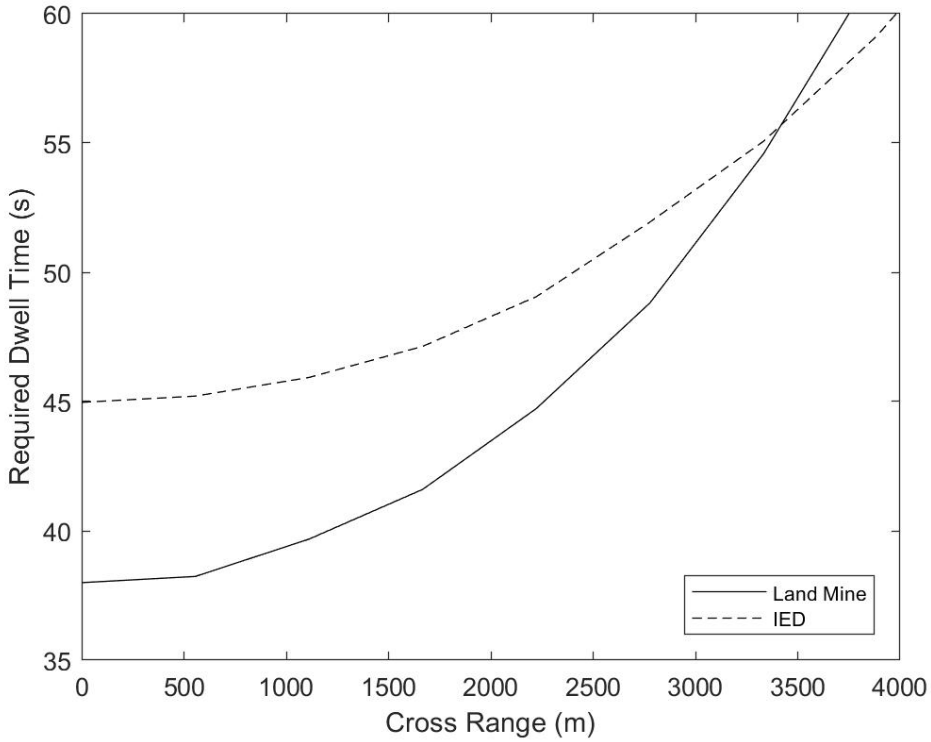

Figure 26. Simulation Results for a Seoul Climate, Hazy Weather, 7 km Platform Altitude, 10 kW Output Power Engagement.

F. CONCLUSIONS

It is feasible to engage and defeat ground ordnance using an airborne solid-state laser. At a platform altitude of 1 km, these simulations indicate that all three tested output powers are capable of achieving autoignition conditions in both climates, across all weather profiles, and against each target type. The most restrictive variable is weather, which effectively limits the platform altitude to the cloud layer during precipitous weather. Additionally, in order to defeat all three target types in clear or hazy weather and in either climate, the minimum required output power increases to 5 kW for 4 km platform altitude engagements and 10 kW for 7 km platform altitude engagements.

The concept of using UAV-mounted solid-state lasers to defeat ground ordnance bears utility. As an example, the IPG Photonics YLS-3000-SM system produces a similar beam to the one simulated in this research with an output power of 10 kW and contained in a compact 0.95 m^3 package [48]. A similar model listed by the company weighs less than 380 pounds and has a published wall-plug efficiency greater than 50% [44]. This means that the system could be operated with a power source that outputs an average of 20 kW. While these SWaP requirements are too large for smaller UAVs such as the RQ-7B Shadow, they do not supersede the capabilities of mid-size UAVs such as the MQ-1C Gray Eagle, which has a payload capacity of 1,075 pounds [49]. This would enable current U.S. Army forces to maintain a responsive airborne ordnance-clearing asset at the division echelon.

There are many opportunities for expansion of this research. The diffusion of heat to achieve autoignition is just one defeat mechanism particular to a specific target type. Different target types with other defeat mechanisms should be studied in order to grasp the full utility of airborne laser systems. Additionally, expanding the selection of platforms beyond UAVs could create possibilities with regard to increased SWaP availability. Rotary and fixed-wing aircraft could theoretically carry laser systems with greater output power, which in turn increases the feasibility of defeating different target types. As solid-state laser systems continue to become more compact and powerful, it is highly likely that airborne laser weapons will become a fixture on future battlefields.

THIS PAGE INTENTIONALLY LEFT BLANK

APPENDIX. MATLAB CODE

A. HEAT DIFFUSION SIMULATION

```
close all;
% overall properties (cylindrical symmetry)
radius = 0.1;          % [m]
height = 0.1;          % [m]
T0 = 300;              % initial (ambient) temperature [K]
Texplode = 1e5;        % explosion threshold temperature [K]

% outer casing properties
thickness = 0.005;     % [m]
rho1 = 959;            % density [kg/m^3]
k1 = 0.43;             % thermal conductivity [W/(m*K)]
cp1 = 2000;            % heat capacity [J/(kg*K)]

% explosive properties
rho2 = 1800;           % density [kg/m^3]
k2 = 0.29;             % thermal conductivity [W/(m*K)]
cp2 = 2093;            % heat capacity [J/(kg*K)]
Qd = 2.09e6;           % heat of decomposition [J/kg]
Ea = 1.99e5;           % activation energy [J/mol]
Ze = 10^18.5;          % characteristic reaction rate [1/s]

% numerical properties
Hmax = 0.005;          % max mesh size [m]
nt = 500;              % number of time steps to save
RelTol = 0.01;         % relative tolerance (larger = faster but less accurate)
trun = 120;            % total time simulation will run [s]
tengage = trun;        % maximum desired engagement time (must equal trun) [s]

% create model object
thermalModelT = createpde('thermal','transient');
thermalModelT.SolverOptions.RelativeTolerance = RelTol;

% define geometry
r1 = [3, 4, 0, radius, radius, 0, -0.5*height, -0.5*height, 0.5*height, 0.5*height];
r2 = [3, 4, 0, radius-thickness, radius-thickness, 0, -0.5*height+thickness,...
    -0.5*height+thickness, 0.5*height-thickness, 0.5*height-thickness];
g = decsg([r1; r2]','R1+R2',['R1'; 'R2']');
geometryFromEdges(thermalModelT,g);

% plot geometry (for edge, face labeling)
%figure
%pdegplot(thermalModelT,'EdgeLabels','on','FaceLabels','on');

% mesh generation
generateMesh(thermalModelT,'Hmax',Hmax);

%pnodes = thermalModelT.Mesh.Nodes;
%indices = pnodes(2,:) < 0;%0.5*height-thickness;

% plot mesh (for diagnostics)
%figure
%pdeplot(thermalModelT);

% assign material properties (outer casing)
k1Func = @(region,state) k1*region.x;
cp1Func = @(region,state) cp1*region.x;
thermalProperties(thermalModelT,'Face',1,'ThermalConductivity',k1Func,...
                                'MassDensity',rho1,...
                                'SpecificHeat',cp1Func);
```

```
% assign material properties (explosive)
k2Func = @(region,state) k2*region.x;
cp2Func = @(region,state) cp2*region.x;
q2Func = @(region,state) Qdot(state,region,Ea,rho2,Qd,Ze);
thermalProperties(thermalModelT,'Face',2,'ThermalConductivity',k2Func,...
                                'MassDensity',rho2,...
                                'SpecificHeat',cp2Func);
internalHeatSource(thermalModelT,q2Func,'Face',2);

% initial conditions
thermalIC(thermalModelT,T0);

clear range;
clear tdwell;
q = 1;
while q <= gridRt

    % laser properties
    Ipk = ANCHOROutput.IrrLinearArray(q,1);          % peak irradiance from ANCHOR [W/m^2]
    wtot = ANCHOROutput.Waist_total_longterm(q,1);   % rms width from ANCHOR [m]
    Reflect = 0.1;                                   % surface reflection coefficient

    % boundary condition(s)
    heatFluxFunc = @(region,state) Ipk*(1-Reflect)*exp(-(region.x).^2./wtot^2).*region.x;
    thermalBC(thermalModelT,'Edge',3,'HeatFlux',heatFluxFunc);

    % run model
    tlist = linspace(0,trun,nt);
    S = solve(thermalModelT,tlist);

    % plot final results
    if max(S.Temperature(:))> Texplode
        Tmax = 0;
        it = 1;
        while Tmax < Texplode
            it = it+1;
            Tmax = interpolateTemperature(S,0,0,it);
            Tmax = max(Tmax(:));
        end

        %figure
        %pdeplot(thermalModelT,'XYData',S.Temperature(:,it),'Contour','off');
        %hold on;
        %pdegplot(thermalModelT);
        %title(strcat('time=',num2str(tlist(it)), 's'));
        %hold off;

        %figure
        %pdeplot(thermalModelT,'XYData',S.Temperature(:,it-1),'Contour','off');
        %hold on;
        %pdegplot(thermalModelT);
        %title(strcat('time=',num2str(tlist(it-1)), 's'));
        %caxis([0 2500]);

        %figure
        %pdeplot(thermalModelT,'XYData',S.Temperature(:,end),'Contour','off');
        %hold on;
        %pdegplot(thermalModelT);
        %title(strcat('time=',num2str(tlist(end)), 's'));

    else
        disp('Time limit exceeded...increasing time step');
        if tlist(end) > 60
            break;
        end
        trun = 2*tlist(end);
        continue;
```

```
    end
    range(1,q) = (q-1)*((Rtmax-Rtmin)/(gridRt-1));
    tdwell(1,q) = tlist(it);
    if tlist(it) > 60
        break;
    end
    q = q+1;
end

% plot cross range versus required dwell time
figure
plot(range,tdwell,'k');
hold on;
xlabel('Cross Range (m)');
ylabel('Required Dwell Time (s)');
```

B. ARRHENIUS HEAT SOURCE FUNCTION

```
function [qdot] = Qdot(state,region,Ea,Rho,Q,Ze)
% QDOT Calculates temperature dependent heat source

R = 8.314;     % ideal gas constant [J/(mol*K)]

if isnan(state.u)
    qdot = NaN(size(region.x));
    return;
else
    qdot = Rho*Q*Ze*exp(-Ea./(R*state.u));
end

maxQ = 1e15;
if max(qdot(:))>maxQ
    qdot = maxQ*ones(size(region.x));
end

qdot = qdot.*region.x;
end
```

THIS PAGE INTENTIONALLY LEFT BLANK

LIST OF REFERENCES

[1] W. H. McMichael, "IED casualties in Iraq drop sharply," *Air Force Times*, Sep. 29, 2008. [Online]. Available: http://libproxy.nps.edu/login?url=https://search.proquest.com.libproxy.nps.edu/docview/1010942507?accountid=12702

[2] G. P. Perram, S. J. Cusumano, R. L. Hengehold, and S. T. Fiorino, *Introduction to Laser Weapon Systems*, 1st ed. Albuquerque, NM, USA: Directed Energy Professional Society, 2010.

[3] I. Vincent, "Afghanistan dotted with millions of land mines: Terrorists' weapon," *National Post*, Oct. 3, 2003. [Online]. Available: http://libproxy.nps.edu/login?url=https://search.proquest.com.libproxy.nps.edu/docview/330081196?accountid=12702

[4] Anonymous, "High energy laser successfully destroys mortars in flight," *Defense Daily International*, vol. 5, no. 32, pp. 1, Aug. 27, 2004. [Online]. Available: http://libproxy.nps.edu/login?url=https://search.proquest.com.libproxy.nps.edu/docview/217308652?accountid=12702

[5] W. Matthews, "Defense tech: Pinpoint Defense," *The Officer*, vol. 87, no. 4, pp. 50–53, Jul., 2011. [Online]. Available: http://libproxy.nps.edu/login?url=https://search.proquest.com.libproxy.nps.edu/docview/884788307?accountid=12702

[6] "Boeing YAL-1," *Wikipedia*. Accessed Apr. 14, 2018. [Online]. Available: https://en.wikipedia.org/wiki/Boeing_YAL-1

[7] S. Brady, "US to deploy new Gray Eagle attack drone system in South Korea," *Stars and Stripes*, Mar. 13, 2017. [Online]. Available: https://www.stripes.com/news/us-to-deploy-new-gray-eagle-attack-drone-system-in-south-korea-1.458364#gallery

[8] J. R. Cook, "High-energy laser weapons since the early 1960s," *Optical Engineering*, vol. 52, no. 2, Feb., 2013. [Online]. doi: 10.1117/1.OE.52.2.021007

[9] J. Horkovich, "Directed energy weapons: Promise & reality," presented at the 37th AIAA Plasmadynamics and Lasers Conference, San Francisco, CA, USA, Jun. 5–8, 2006.

[10] R. Scott, "Parting shot: AN/SEQ-3 Laser Weapon System," *Jane's International Defence Review*, Dec. 22, 2015. [Online]. Available: http://janes.ihs.com.libproxy.nps.edu/InternationalDefenceReview/Display/1759036

[11] H. Simoes, “Navy encouraged by performance of laser system on USS *Ponce*,” *Stars and Stripes*, Dec. 6, 2014. [Online]. Available: https://www.stripes.com/news/navy-encouraged-by-performance-of-laser-system-on-uss-ponce-1.317775#gallery

[12] S. R. Gourley, “Zeus-Humvee Laser Ordnance Neutralization System,” *Army*, vol. 54, no. 12, pp. 51–52, Dec., 2004. [Online]. Available: http://libproxy.nps.edu/login?url=https://search.proquest.com.libproxy.nps.edu/docview/237084034?accountid=12702

[13] “ZEUS-HLONS (HMMWV Laser Ordnance Neutralization System),” *Wikipedia*. Accessed Apr. 14, 2018. [Online]. Available: https://en.wikipedia.org/wiki/ZEUS-HLONS_(HMMWV_Laser_Ordnance_Neutralization_System)

[14] G. Whitty, “Explosive ordnance disposal: New threats, new responses,” *Military Technology*, vol. 25, no. 12, pp. 78–83, Dec. 2001. [Online]. Available: https://search.proquest.com.libproxy.nps.edu/docview/199031941/fulltext/6BF3B77C2E314B53PQ/1?accountid=12702

[15] J. Morgan, “EOD: Defusing the situation,” *U.S. Air Forces Central Command*, Jul. 26, 2013. [Online]. Available: http://www.afcent.af.mil/News/Article/500784/eod-defusing-the-situation/

[16] J. Doubleday, “Laser, railgun programs established at Navy acquisition offices,” *Inside the Pentagon’s Inside Missile Defense*, vol. 23, no. 5, Mar. 1, 2017. [Online]. Available: https://search.proquest.com.libproxy.nps.edu/docview/1872758287/fulltext/4FF075CAD00344A7PQ/1?accountid=12702

[17] L. Giangreco, “Air Force aims to complete high-energy laser demonstration by 2020,” *Inside the Pentagon’s Inside Missile Defense*, vol. 21, no. 16, Aug. 4, 2015. [Online]. Available: https://search.proquest.com.libproxy.nps.edu/docview/1701519846/fulltext/488E1A9BDE574F4DPQ/1?accountid=12702

[18] M. J. Lavan and J. J. Wachs, “U.S. Army High Energy Laser (HEL) technology program,” in *Proc. of SPIE 8187, Technologies for Optical Countermeasures VIII*, 2011. [Online]. doi: 10.1117/12.903729

[19] J. Joyce, “Afghan Commandos, USSOF seize insurgent weapons inventory,” *War on Terror News*, Apr. 25, 2011. [Online]. Available: http://waronterrornews.typepad.com/home/2011/04/special-forcesafghan-commandos-take-out-ied-factory-in-helmand.html#more

[20] R. Weinheimer, “Properties of selected high explosives,” presented at the 27th International Pyrotechnics Seminar, Grand Junction, CO, USA, Jul. 16–21, 2000.

[21] Collaborative Ordnance Data Repository. Object name U.S.S.R. BOMB, HEAT, PTAB-2.5M. [Online]. Available: https://ordata.info/ordnance?id=4979. Accessed Apr. 14, 2018.

[22] Collaborative Ordnance Data Repository. Object name U.S.S.R. LANDMINE, AT, TM-83. [Online]. Available: http://ordata.info/ordnance?id=3959. Accessed Apr. 14, 2018.

[23] S. Venugopalan, *Demystifying Explosives—Concepts in High Energy Materials*, 1st ed. Amsterdam, Netherlands: Elsevier, 2015.

[24] N. Kubota, *Propellants and Explosives: Thermochemical Aspects of Combustion*, 3rd ed. Weinheim, Germany: Wiley-VCH, 2015.

[25] H. DaCosta, *Rate Constant Estimation for Thermal Reactions Methods and Applications*, 1st ed. Hoboken, NJ, USA: Wiley, 2012.

[26] N. E. Henriksen and F. Y. Hansen, *Theories of Molecular Reaction Dynamics: The Microscopic Foundation of Chemical Kinetics*. New York, NY, USA: Oxford University Press, 2008.

[27] C. D. Boley and A. M. Rubenchik, "Modeling of antimortar lethality by a solid-state heat-capacity laser," *Journal of Directed Energy*, vol. 2, no. 2, pp. 97–106, 2006.

[28] R. Arieli, "The parameters which determines the beam divergence," The Laser Adventure. Accessed April 26, 2018. [Online]. Available: https://perg.phys.ksu.edu/vqm/laserweb/Ch-7/F7s2t2p5.htm

[29] W. Jing, W. Yang, X. Wang, and H. Jiang, "Research on solving laser beam quality factor M^2 with normal equations," in Elect. and Cont. Eng. 2010 Intl. Conf., Wuhan, China, 2010. [Online]. doi: 10.1109/iCECE.2010.434

[30] C.R. Fussman, "High energy laser propagation in various atmospheric conditions utilizing a new, accelerated scaling code," M.S. thesis, Dept. of Phy., NPS, Monterey, CA, USA, 2014. [Online]. Available: https://calhoun.nps.edu/bitstream/handle/10945/42628/14Jun_Fussman_Chris.pdf;sequence=3

[31] E. Penrod, "Former EPA leader defends actions on Utah haze, ozone," The Salt Lake Tribune, May 19, 2017. [Online]. Available: http://archive.sltrib.com/article.php?id=5306391&itype=CMSID

[32] P. E. Nielsen, *Effects of Directed Energy Weapons*. Albuquerque, NM, USA: Directed Energy Professional Society, 2009.

[33] P. Sprangle, J.R. Peñano, A. Ting, and B. Hafizi, “Propagation of high-energy lasers in a maritime atmosphere,” NRL Rev., pp. 59-67, 2004. [Online]. Available: https://www.nrl.navy.mil/content_images/2004Review.pdf

[34] A. Tunick, N. Tikhonov, M. Vorontsov, and G. Carhart, “Characterization of optical turbulence (*Cn2*) data measured at the ARL A_LOT facility,” ARL, Adelphi, MD, USA, Rep. ARL-MR-625, 2005. [Online]. Available: https://www.arl.army.mil/arlreports/2005/ARL-MR-625.pdf

[35] V. Sacek, “Atmospheric turbulence,” Notes on Amateur Telescope Optics, June, 2015. [Online]. Available: http://www.telescope-optics.net/induced.htm

[36] J. R. Cook, “Atmospheric propagation of high energy lasers and applications,” in AIP Conf. Proc., 2005. [Online]. doi: https://doi.org/10.1063/1.1925132

[37] B. MacEvoy, “The location of turbulence,” Astronomical Seeing, November 26, 2013. [Online]. Available: https://www.handprint.com/ASTRO/seeing1.html

[38] Material Thermal Properties Database. [Online]. Available: https://ncfs.ucf.edu/burn_db/Thermal_Properties/material_thermal.html

[39] J. Zinn and C. L. Mader, “Thermal Initiation of Explosives,” Jrnl. of App. Phy., vol. 31, no. 2, pp. 323-328, Feb. 1960. [Online]. doi: 10.1063/1.1735565

[40] The World Factbook. Object name Korea, South. [Online]. Available: https://www.cia.gov/library/publications/the-world-factbook/geos/ks.html. Accessed Apr. 26, 2018.

[41] The World Factbook. Object name Afghanistan. [Online]. Available: https://www.cia.gov/library/publications/the-world-factbook/geos/af.html. Accessed Apr. 26, 2018.

[42] The Office of the Director, Operational Test and Evaluation, “Shadow 200 tactical unmanned aerial vehicle (TUAV) system,” Washington, DC, USA, 2002. [Online]. Available: http://www.dote.osd.mil/pub/reports/FY2002/pdf/army/2002Shadow200TUAV.pdf

[43] “RQ-4 Global Hawk,” U.S. Air Force, October, 2014. [Online]. Available: http://www.af.mil/About-Us/Fact-Sheets/Display/Article/104516/rq-4-global-hawk/

[44] “YLS-ECO, 1-10 kW,” IPG Photonics. Accessed April 26, 2018. [Online]. Available: https://www.ipgphotonics.com/en/products/lasers/high-power-cw-fiber-lasers/1-micron/yls-eco-1-10-kw

[45] D. H. Tolsted, S. G. O'Brien, and G. T. Vaucher, "An atmospheric turbulence profile model for use in army wargaming applications I," ARL, White Sands Missile Range, NM, USA, Rep. ARL-TR-3748, 2006. [Online]. Available: https://www.arl.army.mil/arlreports/2006/ARL-TR-3748.pdf

[46] "Typical engineering properties of high density polyethylene," INEOS Holdings Limited. Accessed April 28, 2018. [Online]. Available: https://www.ineos.com/globalassets/ineos-group/businesses/ineos-olefins-and-polymers-usa/products/technical-information--patents/ineos-typical-engineering-properties-of-hdpe.pdf

[47] "Clouds," National Geographic. Accessed April 28, 2018. [Online]. Available: https://www.nationalgeographic.com/science/earth/earths-atmosphere/clouds/

[48] "YLS-SM, 1-10 kW," IPG Photonics. Accessed April 28, 2018. [Online]. Avalable: https://www.ipgphotonics.com/en/products/lasers/high-power-cw-fiber-lasers/1-micron/yls-sm-1-10-kw

[49] "Gray Eagle UAS," General Atomics Aeronautical. Accessed April 28, 2018. [Online]. Available: http://www.ga-asi.com/gray-eagle

THIS PAGE INTENTIONALLY LEFT BLANK

INITIAL DISTRIBUTION LIST

1. Defense Technical Information Center
   Ft. Belvoir, Virginia

2. Dudley Knox Library
   Naval Postgraduate School
   Monterey, California